Available online at www.sciencedirect.com

ScienceDirect

Geochimica et Cosmochimica Acta 209 (2017) 296–319

Geochimica et Cosmochimica Acta

www.elsevier.com/locate/gca

Calcium and strontium isotope fractionation in aqueous solutions as a function of temperature and reaction rate; I. Calcite

Mahmoud AlKhatib, Anton Eisenhauer *

GEOMAR Helmholtz-Zentrum für Ozeanforschung Kiel, Wischhofstr. 1-3, 24148 Kiel, Germany

Received 10 February 2016; accepted in revised form 22 September 2016; Available online 7 October 2016

Abstract

In order to study Strontium (Sr) partitioning and isotope fractionation of Sr and Calcium (Ca) in calcite we performed precipitation (T) experiments decoupling temperature and precipitation rate (R^*). Calcite was precipitated at 12.5, 25.0 and 37.5 °C by diffusing NH_3 and CO_2 gases into aqueous solutions closely following the experimental setup of Lemarchand et al. (2004). The precipitation rate (R^*) for every sample was determined applying the initial rate method and from the specific surface area of almost all samples for each reaction. The order of reaction with respect to Ca^{2+} ions was determined to be one and independent of T. However, the order of reaction with respect to HCO_3^- changed from three to one as temperature increases from 12.5, 25 °C and 37.5 °C. Strontium incorporated into calcite (expressed as $D_{Sr} = [Sr/Ca]_{calcite}/[Sr/Ca]_{solution}$) was found to be R^* and T dependent. As a function of increasing R^* the $\Delta^{88/86}$Sr-values become more negative and as temperature increases the $\Delta^{88/86}$Sr values also increase at constant R^*. The D_{Sr} and $\Delta^{88/86}$Sr-values are correlated to a high degree and depend only on R^* being independent of temperature, complexation and varying initial ratios. Latter observation may have important implications for the study of diagenesis, the paleo-sciences and the reconstruction of past environmental conditions. Calcium isotope fractionation ($\Delta^{44/40}$Ca) was also found to be R^* and T dependent. For 12.5 and 25.0 °C we observe a general increase of the $\Delta^{44/40}$Ca values as a function of R^* (Lemarchand et al. type behavior, Lemarchand et al. (2004)). Whereas at 37.5 °C a significant decreasing $\Delta^{44/40}$Ca is observed relative to increasing R^* (Tang et al. type behavior, Tang et al. (2008)). In order to reconcile the discrepant observations we suggest that the temperature triggered change from a Ca^{2+}-NH_3-aquacomplex covalent controlled bonding to a Ca^{2+}-H_2O-aquacomplex van-der-Waals controlled bonding caused the change in sign of the $R^* - \Delta^{44/40}$Ca slope due to the switch of an equilibrium type of isotope fractionation related to the covalent bonding during lower temperatures to a kinetic type of isotope fractionation at higher temperatures. This is supported by the observation that the $\Delta^{44/40}$Ca ratios tend to depend on the [Ca]:[DIC] ratio at 12.5 and 25 °C but is highly independent at 37.5 °C. Our observations imply the chemical fluid composition and temperature dependent complexation controls the amount and direction of Ca isotope fractionation in contrast to the Sr isotopes which do not show any change of its fractionation behavior as a function of complexation in the liquid phase.

Keywords: Calcium; Strontium; Calcium isotopes; Strontium isotopes; Calciumcarbonate; Precipitation rate; Temperature

1. INTRODUCTION

Carbonate minerals contribute to a large extent to the global carbon budget (Morse and Mackenzie, 1990), play an important role in adsorption and desorption processes in the environmental systems (e.g., Langmuir, 1997) and control long term climate change (Berner, 2004). Calcium carbonate ($CaCO_3$) is usually produced by biogenic and inorganic precipitation processes from aqueous solutions and has three major polymorphs aragonite, calcite and vaterite of which calcite is the most abundant one.

* Corresponding author. Fax: +49 431 6002928.
E-mail address: aeisenhauer@geomar.de (A. Eisenhauer).

http://dx.doi.org/10.1016/j.gca.2016.09.035
0016-7037/

Inorganic precipitation of Ca carbonate is usually induced by increasing the concentration of one of the reactants until the aqueous solution becomes supersaturated with these ions (c.f. Niedermayr et al., 2013). Inorganic natural calcite formation is usually related to evaporate and carbonate cements in sediments. In contrast biogenic calcite is produced along different ways of biomineralisation by uni- and multi-cellular calcifying organisms like coccoliths, foraminifera, calcareous sponges, brachiopods (c.f. Atkins and De Paulla (2006)). The calcite mineral is not pure (Garrels and Christ, 1965) rather contains a variety of trace elements mostly other divalent positively charged alkaline-earth elements like Magnesium (Mg), Strontium (Sr), Barium (Ba), but also other elements like Lithium (Li), Boron (B), Cadmium (Cd), Uranium (U), Thorium (Th) and others. The enrichment of these trace elements relative to Ca reflects their specific environmental conditions in the adjacent bulk solution at the time of formation (Morse and Bender, 1990) and may eventually be used as a chemical indicator of past environmental conditions (proxy). These conditions include the composition of solutions, concentration of dissolved trace elements, T, pH, salinity and the degree of saturation of these minerals. In calcite beside Mg the most important trace element is Sr. For example foraminifera which are responsible for about 20% of the total calcite sediments and 5 to 10% of the total sediments in the marine environments form the main sink of Sr (Böhm et al., 2012; Vollstaedt et al., 2014). In addition, the Sr/Ca ratio measured in aragonite has been widely used in paleo-oceanographic studies to estimate past sea surface temperatures (SST) (e.g., Smith et al., 1979; Rosenthal et al., 1997; Gagan et al., 1998). This elemental ratio is also used to understand the composition of past seawater, to study the diagenetic reactions that involve carbonate sediments (e.g., Lorens, 1981; Baker et al., 1982; Mucci and Morse, 1983; Richter and Liang, 1993; Banner, 1995; Humphrey and Howell, 1999; Malone and Baker, 1999). The Sr/Ca ratio in biogenic calcite was also correlated to both nutrient level and growth rate (e.g., Weinbauer and Velimirov, 1995; Stoll and Schrag, 2000; Stoll et al., 2002a,b).

In addition numerous experimental studies have been carried out to evaluate effects of different environmental conditions (T, R^*, pH and salinity changes) on Sr incorporation into calcite. Earlier culturing experiments using foraminifera and coccoliths (e.g., Lea et al., 1999; Stoll and Schrag, 2000; Stoll et al., 2002a,b) suggested that Sr/Ca ratios increase (corresponding to an increasing Sr partitioning coefficient (D_{Sr}) = ($[Sr/Ca]_{calcite}/[Sr/Ca]_{solution}$) with increasing calcite R^* and/or increasing temperature. Similar results were shown by experiments to examine inorganic calcite precipitation of (Lorens, 1981; Tesoriro and Pankow, 1996; Huang and Fairchild, 2001; Nehrke et al., 2007; Tang et al., 2008a, 2012; Gabitov et al., 2014). Although the slope and general behavior is similar in all previous experiments the gradients and values mostly differ depending on the experimental conditions of each single experiment. In particular only Tang et al., 2008a studied the combined effect of temperature and R^*. They found at constant rate of precipitation as temperature increase D_{Sr} values decrease. Furthermore, Tang et al., 2012 studied the effect of salinity parallel to the effect of rate of precipitation and found that it has an insignificant effect on the D_{Sr} values. Also for biogenic calcite and experimental transformation of aragonite to calcite a positive or insignificant T dependence was observed (Katz et al., 1972; Jacobson and Usdowski, 1976; Baker et al., 1982; Stoessell et al., 1987; Lea et al., 1999; Humphrey and Howell, 1999; Malone and Baker, 1999; Stoll et al., 2002a,b).

According to our knowledge there is only one study in the literature dealing with Sr isotope fractionation (expressed as $\Delta^{88/86}Sr$) between experimentally precipitated calcite and aqueous solution presented earlier by our group (Böhm et al., 2012). The authors found at 25 °C that Sr isotope fractionation in calcite is strongly dependent on R^*, as rate increase more lighter Sr isotopes are incorporated into calcite corresponding to increasingly lower $\Delta^{88/86}Sr_{calcite\text{-}aq}$ values. They also compared these results with Sr isotope fractionation in biogenic foraminiferal calcite samples and interpreted the strong Sr isotope fractionation of these samples to be due to calcification at high R^*.

Nevertheless the literature values available concerning Ca isotopic fractionation between calcite and aqueous solution are discrepant to a certain extent. Tang et al., 2008b found that Ca isotope fractionation is both R^* and T dependent, as R^* increases more lighter Ca isotopes are incorporated into calcite corresponding to increasingly lower $\Delta^{44/40}Ca_{calcite\text{-}aq}$ values. Concerning T the $\Delta^{44/40}Ca_{calcite\text{-}aq}$ values increase as a function of T at constant R^*. In contrast earlier experiments by Lemarchand et al. (2004) found that as R^* increase more heavier Ca isotopes are incorporated into calcite corresponding to increasingly higher $\Delta^{44/40}Ca_{calcite\text{-}aq}$ values. The latter discrepant observation of lower and higher $\Delta^{44/40}Ca_{calcite\text{-}aq}$ values as a function of increasing R^* became the impetus for this study to repeat the original experiment of Lemarchand et al. (2004).

In this study we closely followed the original experimental setup of Lemarchand and precipitated calcite from aqueous ammonium buffered solution through spontaneous decomposition of solid ammonium carbonate ($(NH_4)_2CO_3$) into aqueous solutions containing Ca^{2+} ions. This experimental setup allows us to precipitate calcite with different R^* at three selected temperatures (~12.5, ~25.0 and ~37.5 °C). The goal of this experimental approach is to do a whole kinetic study in order to evaluate how R^*, T and Sr/Ca ratios in the precipitating solutions will affect the D_{Sr} values, Sr isotopic fractionation ($\Delta^{88/86}Sr_{calcite\text{-}aq}$) and Ca isotopic fractionation ($\Delta^{44/40}Ca_{calcite\text{-}aq}$). Finally, we intend to provide a qualitative model in order to reconcile the discrepant results concerning earlier observations on Ca isotopic fractionation.

2. MATERIAL AND METHODS

2.1. Materials and experimental setup

The original experimental setup of this method to precipitate Ca carbonates ($CaCO_3$) was described initially by (Gruzensky, 1967), later used by (Paquette and Reeder, 1990, 1995; Hemming et al., 1995; Lemarchand et al.,

2004) and finely by (Gabitov, 2013) to precipitate calcite, high-Mg calcite and aragonite. In this work we modified the sealed chamber with a copper tubing coil to control the temperature inside as it is shown in Fig. 1.

Two main sets of solutions were prepared to produce calcite in an ammonium buffered solutions (NH_4/NH_3) at three different temperatures 12.5, 25.0 and 37.5 (±0.2 °C). The first set is composed of 0.395 M NH_4Cl, 10.0 mM $CaCl_2$ and 0.10 mM $SrCl_2$. The second solution shows the same composition except for $SrCl_2$ to be 0.050 mM $SrCl_2$. In order to verify differences in chemical composition three solutions were prepared differently following the original experiment by Lemarchand et al. (2004) which either contained 15 or 150 mM [Ca], respectively: in reaction no. 4 the reacting solution is composed of 0.395 M NH_4Cl, 19.84 mM $CaCl_2$ and 0.11 mM $SrCl_2$, in reaction no. 7 reacting solution is composed of 0.395 M NH_4Cl, 149.00 mM $CaCl_2$ and $SrCl_2$. Finally in reaction no. 8 reacting solution is composed of 0.395 M NH_4Cl, 148.42 mM $CaCl_2$ and 1.5 mM $SrCl_2$. Ammoniumhydrochlorid (NH_4Cl) is used here to buffer the solution and to adjust the ionic strength of the solutions. All the chemicals are ACS grade of Merck and all aqueous solutions were prepared using deionized water (18.2 MΩ).

In this technique 400–550 ml of NH_4Cl-$CaCl_2$-$SrCl_2$-solution and the solid $(NH_4)_2CO_3$ (ammonium carbonate) are contained within the sealed reacting chamber. In all experiments the reacting solution is stirred with a magnetic stirrer at 300 rounds per minute. Ammonium carbonate decomposes spontaneously and produces an ammonia/carbon dioxide atmosphere within the chamber by the reaction:

$$(NH_4)_2(CO_3)_{(S)} \leftrightarrow 2NH_{3(g)} + CO_{2(g)} + H_2O_{(g)} \quad (1)$$

Ammonia and carbon dioxide gases diffuse and dissolve in the experimental solution increasing pH and alkalinity by the following reactions

$$NH_{3(g)} + H_2O_{(g)} \leftrightarrow NH_4^{+(aq)} + OH^-_{(aq)} \quad (2)$$

$$CO_{2(g)} + H_2O_{(g)} \leftrightarrow CO_{2(aq)} \quad (3)$$

$$CO_{2(aq)} + H_2O_{(aq)} \leftrightarrow H_2CO_3 \quad (4)$$

$$H_2CO_3 \leftrightarrow HCO^-_{3(aq)} + H^+_{(aq)} \quad (5)$$

$$HCO^-_{3(aq)} \leftrightarrow CO_{3(aq)^{2-}} + H^+ \quad (6)$$

The overall spontaneous reaction of the steps (1) to (6) is:

$$(NH_4)_2(CO_3)_{(S)} \rightarrow 2NH^+_{4(aq)} + CO_{3(aq)^{2-}}$$

The result of these reactions is the supersaturation of the reacting solution with respect to calcite. The dynamic of the reaction was monitored by a WTW 3100 pH meter which was standardized against buffer solutions of pH 4, 7 and 10 before each single experiment. This pH meter connected to a computer monitors the pH values and the temperature of the solution online (see Fig. 1) continuously and stores the measured data in an excel sheet. We controlled the rate of reaction as well as the time needed to reach the precipitation point by the quantity, the surface area of the granules of ammonium carbonate and by the surface area through which the gases diffuse. For example for slow reaction rates we use 5–10 g of ammonium carbonate with a radius of about one centimeter. In this case we found the rate of reaction ranging between 1.2 and 3.0 μmol/m^2·h and the time needed for precipitation to start range between 3 and 12 days depending on individual reaction temperature. To

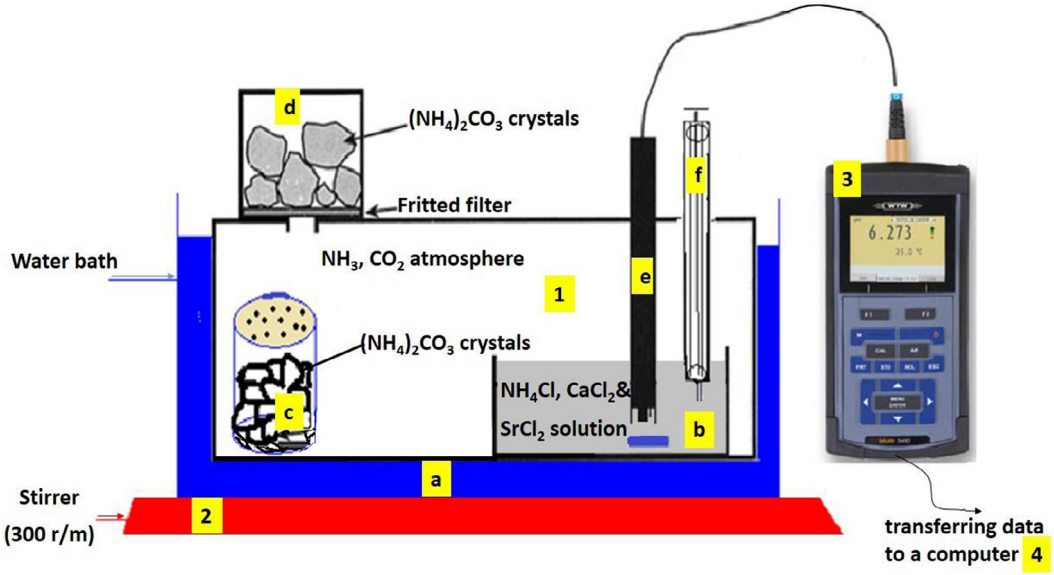

Fig. 1. Schematic design of the experimental setup: (1) the reaction chamber which is a sealed plastic container consisting of a copper tubing (a) where water is circulating to keep a constant temperature, (b) a beaker that contains the reacting solution, (c) a beaker that contains some ammonium carbonate granules that decompose spontaneously to provide ammonia and carbon dioxide gases, (d) fritted filter funnel that also contains some ammonium carbonate granules, (e) pH and temperature sensors, (f) syringe to withdraw samples from the reacting solution, (2) magnetic stirrer, (3) pH meter and (4) computer recording the measured data in an excel sheet.

accelerate the reactions we put additional beaker containing solid ammonium carbonate (different quantities and different particle size) inside the reacting chamber. This beaker was covered with parafilm and perforated with a distinct number of holes. In certain cases the beaker was not covered at all, then the rate of reaction increased ranging from 4.4 to 33.2 μmol/m^2·h and the time needed to start precipitation ranging between 24.7 and 3.2 h depending on the temperature of individual reaction.

During the experiment the chemical evolution of the reacting solution was monitored by sampling 2–5 ml at distinct time intervals ranging between 5 and 30 min depending on the reaction time to be analyzed later. We allowed each reaction to run for a certain period of time depending on its rate then stopped it by removing the reacting solution from the sealed chamber and filter the solution as fast as possible by vacuum filtration through a regenerated cellulose filter paper with a pore size of 0.2 μm. Then the solid was washed with deionized water (18.2 MΩ) and mixed with a small volume of pure ammonium hydroxide solution to make it slightly alkaline. Furthermore, the filter was finally washed with pure ethanol in order to remove any adsorbed $CaCl_2$ or/and $SrCl_2$ aqueous solutions on the surface of the crystals.

2.2. Analysis

2.2.1. Dissolved inorganic carbon (DIC)

In order to calculate DIC, the total alkalinity (TA) of each experiment through the whole period of reaction has to be calculated. We did this by titrating 0.2 ml of the reaction mixture at different intervals of time during the precipitation reaction against 0.02 N HCl (dilution of ME RCK-Titrisol-solution™). This HCl solution is initially standardized against IAPSO seawater (Certified alkalinity of 2.325 mM) using a micro titration apparatus Metrohm 665 Dosimat equipped with a titration vessel of 7 cm. During the titration the sample is degassed with nitrogen continuously to remove any CO_2. The indicator used in this titration is prepared from two solutions. Solution 1: about 1–32 mg Methyl Red (or 37 mg of sodium salt of Methyl Red) mixed with 1.19 ml of 0.1 M NaOH and dissolved in 80 ml 96% ethanol. Solution 2: about 2–10 mg Methylene Blue dissolved in 10 ml 96% ethanol. Taking 4.8 ml of solution 2 and mixing it with 80 ml of solution 1 to obtain a greenish-brown solution, at the end point of the titration solution becomes pink. In each titration the volume of indicator used was 20 μl added to 4.8 ml of water and 0.2 ml sample. Each sample was titrated three times and the average volume was used to calculate the total alkalinity.

Furthermore the concentration of ammonia (NH_3 aq) in our samples has to be determined and the apparent acid dissociation constant of ammonium chloride in our experimental condition has to be calculated ($K_a = [NH_3]\,[H^+]/[NH_4^+]$; K_a = apparent dissociation constant). The value for K_a had to be determined because only one value for 20 °C was known before. Following this 6 ml aliquot of the mother solution was titrated potentiometrically against 1 M NaOH aq using the micro titration apparatuses. The average volume of the three titration trials was 2.40 ml NaOH. Then the pH of half neutralized mother solution was measured in a thermostat at different temperatures. At each temperature the half neutralized solution was kept at least 30 min in the thermostat in order to reach thermal equilibrium before measuring its pH. The salinity of the reaction mixtures was measured by WTW cond. 3110 set 1.

2.2.2. Elemental analysis

We analyzed the concentrations of Ca and Sr ions in the bulk solutions at different intervals of time during the course of each reaction. Furthermore, after dissolution of the solid carbonate samples the elemental ratio was measured by inductively coupled plasma mass spectrometry (ICP-MS-QP Agilent 7500cx) together with Indium (In) as an internal standard. All samples were diluted in 2% HNO_3 to reach 25.0 ± 2.5 ppm Ca in order to avoid matrix effects. Coral standard JCP-1 was used as a reference material and measured as every fifth sample and in a total of ten times during the course of this study ($N = 10$). The JCP-1 Sr/Ca ratio was calculated to be 8.82 ± 0.02 mmol/mol which matches within error the reported value of 8.84 ± 0.08 mmol/mol of Hathorne et al. (2013). In addition we also measured standard JCT-1 to be 1.693 ± 0.004 mmol/mol which is also in agreement with the value of Hathorne et al. (2013) to be 1.680 ± 0.055 mmol/mol. The average uncertainty for our Sr/Ca mmol/mol ratios are less than 1% and correspond to the 95% confidence level.

2.2.3. Crystalline structure and specific surface area of calcite products

The crystalline structure of the solid products was analyzed by X-ray diffraction and by scanning electron microscope (SEM) CamScan-CS-44, equipped with a secondary electron detector, backscattered electron detector, thermal evaporator Edwards Auto 306 and sputtering-coater EMITECH K550, Au/Pd (80/20). Measurements were performed with an X-ray-diffractometer "D8 Discover" (Bruker AXS). The samples were analyzed in a 2Θ-range from 4° to 90° with a step size of 0.007° and counting time 1.5 s/step using a Cu X-ray radiation source. Software was evaluated by High Score Plus Version 3.0d (3.0.4) by PANalytical. All measurements were carried out at the Geology Department of Kiel University.

2.2.4. Strontium and calcium isotope analysis

Measurements were carried out at the GEOMAR mass spectrometer facilities in Kiel, Germany, with a Thermo-Fisher Triton T1 Thermal-Ionization-Mass-Spectrometer (TIMS). Strontium ($\delta^{88/86}$Sr) and Ca ($\delta^{44/40}$Ca) isotope composition were measured for all solid products as well as for the mother solution of these reactions closely following the procedure as described earlier by Krabbenhöft et al. (2009). At least two isotope measurements have to be performed. One unspiked run (ic-run, isotope composition) and one run with a ^{87}Sr/^{84}Sr-double spike added to the sample solution (id-run, isotope dilution). Sample size was selected to be in the order of 1500 ng of Sr. Spike correction and normalization of the results was carried out as described by Krabbenhöft et al. (2009). During the course

of this project two ic-run and id-run for each sample in each session were measured. For quality control the following standard materials were applied: SRM987 $SrCO_3$ standard from the National institute of standards and technology (NIST), JCp-1 coral standard and IAPSO seawater standard. We report the statistical uncertainties of our measurements as twice the standard deviation of the mean ($2\sigma_{mean} = 2\sigma/n^{0.5}$); where n is the number of measurements. The measured $^{88}Sr/^{86}Sr$ ratios are reported in the common δ-notation relative to NIST SRM987: $\delta^{88/86}Sr\ (‰) = [(^{88}Sr/^{86}Sr)_{sample}/(^{88}Sr/^{86}Sr)_{SRM987} - 1] * 1000$. The blank values of our chromatographic column separations were <0.10 ng Sr as a whole procedure blank in all batches we prepared. The $\delta^{88/86}Sr$-values of column separated SRM987 chemistry was measured in three different batches and has these values (0.00 ± 0.02, 0.018 ± 0.014 and $0.003 \pm 0.005‰$, $n = 4$ for each) showing insignificant deviations from the reference values due to the column separation of the standard. The $\delta^{88/86}Sr$-values of separated IAPSO of our three batches resulted into (0.372 ± 0.006, 0.399 ± 0.001 and $0.392 \pm 0.005‰$, $n = 4$ for each) which compares well with the long term IAPSO average of the instrument measurements $0.391 \pm 0.004‰$, $n = 63$. The $\delta^{88/86}Sr$-values of separated JCP-1 of our three batches respectively (0.188 ± 0.006, 0.200 ± 0.010 and $0.196 \pm 0.004‰$, $n = 4$ for each), while the mean value of measurements carried out by this instrument is ($0.195 \pm 0.003‰$, $n = 87$). The method adopted for Ca isotope measurement follows Heuser et al. (2002) and Böhm et al. (2006), respectively. For each sample to be analyzed 3000 ng of Ca were spiked with 120 µl $^{43}Ca/^{48}Ca$ double spike to correct for isotope fractionation in the mass spectrometer during the course of the Ca isotope analysis. The mixture was evaporated to dryness and then redissolved in 100 µl 0.9 N HCl, this solution was loaded onto ion exchange column (BIO RAD of 800 µl bed volume; cation exchange resin MCI Gel, CK08P, 75–150 µ, Mitsubishi chemical composition) in order to extract the Ca-fraction. After washing the column with water (18.2 MΩ) and then with 1.5 N HCl, sample was loaded to the column, and washed again with 3.5 ml 1.5 N HCl. The Ca-fraction was then eluted after rinsing the column with 9 ml 1.5 N HCl. Then the solution was evaporated to dryness and redissolved in 20 µl 2.5 N HCl. This quantity is enough to load ten filaments to be measured into ten separate runs. Details of the measurement procedure can be found in Heuser et al. (2002) and Böhm et al. (2006). In each run session NIST SRM915a was measured four times, CaF_2 was measured twice (which used as a control standard) and each sample was measured at least five times. The isotopic ratio of each sample as well as CaF_2 was normalized to the mean of the four $^{44}Ca/^{40}Ca$ NIST SRM915a analysis and reported in the common delta notation $\delta^{44/40}Ca\ (‰) = [(^{44}Ca/^{40}Ca)_{sample}/(^{44}Ca/^{40}Ca)_{standard} - 1] * 1000$. The blank values of our chromatographic column separations were <15 ng of Ca as a whole procedure blank in all batches we prepared. The average of $\delta^{44/40}Ca$ of separated NIST SRM915a by column chemistry was measured 12 times in three different batches was $0.02 \pm 0.02‰$, it shows insignificant deviation due to the column separation of the standard. The average of $\delta^{44/40}Ca$ of CaF_2 measured in 20 different runs was $1.4 \pm 0.2‰$ ($n = 40$) which is in absolute agreement with earlier measurements (c.f. Heuser et al., 2005).

We are reporting Sr and Ca fractionation in the big delta notations $\Delta^{88/86}Sr = \delta^{88/86}Sr_{calcite} - \delta^{88/86}Sr_{initial}$ solution and $\Delta^{44/40}Ca = \delta^{44/40}Ca_{calcite} - \delta^{44/40}Ca_{initial}$, respectively. Note, "calcite" denotes to the precipitates and "initial" to the original solution. All Δ-values are corrected for the Rayleigh distillation effect (Zeebe and Wolf-Gladrow, 2003) in order to account for the reservoir effect as shown in the following equation (information about the derivative of Eq. (7) are presented in the Appendix):

$$\alpha_{corrected} = \left(\ln\left[\frac{\Delta f}{1000} + f - \left(\frac{\Delta}{1000}\right)\right]\right) / \ln f \quad (7)$$

where f is the fraction of metal ions remaining in the aqueous solution and α is the isotope fractionation factor defined as ($^{44}Ca/^{40}Ca_{calcite}./^{44}Ca/^{40}Ca_{initial}$)

$$\Delta_{correct\approx}(\alpha_{corrected} - 1) \cdot 1000 \quad (8)$$

In Table 5 the original data (column 16) together with the corrected data (column 17) for Rayleigh fractionation are presented.

Note that the corrections (for more details see in the Appendix Figs. A1 and A2 for the reservoir effect is small (<0.02‰) for Sr but larger for the Ca isotopes (<~0.5‰). We also note that the correction is based on an equation originally designed to describe the cumulative product of a Rayleigh distillation process in a closed system (Zeebe and Wolf-Gladrow, 2003). This is actually an irreversible process and hence may not adequately describe the situation of a growing crystal controlled by reversible processes of precipitation and dissolution occurring at the same time. In this regard the correction as applied here may over simplify the complex processes occurring in our free-drift experiment. For further discussion we will use the corrected values (Table 5, columns 14 and 17) instead of the uncorrected ones (column 13 and 16) being aware that there may be some uncertainties (<0.02‰ for Sr and <~0.5‰ for Ca) in our interpretations.

In order to verify the variability of the fractionation factor α for the $\Delta^{44/40}Ca$ values we plotted them (see Appendix and Fig. A3) as a function of the remaining [Ca] in solution (f) applying the original Eq. 3.1.17 in Zeebe and Wolf-Gladrow (2003). For the calculation of the parameter f the fractionation factor α was calculated from the first data outside the linear part of the precipitation curve. As one can see from Fig. A3 theoretical predictions and experimental data are in general accord. Taken into account that the calculation of f and α was performed from data outside the linear part of the precipitation curve may indicate that the internal variations of the fractionation factor α is relatively small during the experiment (for more details we refer to the Appendix A).

3. RESULTS

The concentrations of NH_3 and NH_4 in our experimental setup are relatively high when compared f.e. with the concentrations used in Tang et al. (2008). Latter fact inhibits the calculations of activity coefficients applying geochemical modeling and the PHREEQC software.

Consequently, all calculations are based on concentrations only.

3.1. pH, total alkalinity and saturation indexes (SI) with respect to calcite, amorphous calcium carbonate (ACC) and strontianite ($SrCO_3$)

The experiment shows that the pH of the solution gradually increase (Fig. 2) as soon as the absorption of the evolved gases (CO_2 and NH_3) into aqueous solution starts until it reaches a maximum value (marked with a red point in Fig. 2) and then decrease slightly after the real precipitation point. The Ca^{2+} -ions react with HCO_3^- but then it is redistributed to CO_3^{2-} which results in a pH drop according to Eq. (9). The start of the precipitation is also characterized by a simultaneous drop of dissolved [Ca] and [Sr] in the solution exactly at this pH.

$$HCO_3^- + Ca^{2+} \leftrightarrow CaCO_{3(s)} + H^+ \quad (9)$$

Throughout the reaction the pH of the reacting solution (when precipitation starts) remains relatively constant (±0.02 units) as well as the temperature of all reactions (±0.2 °C). In the Appendix we show details of calculating acid dissociation constant of ammonium ions (K_a) as function of temperature and molar concentrations of different alkaline species in reacting solutions (NH_3, HCO_3^- and CO_3^{2-}). The results of this part are summarized in Table 1 where SI values are calculated with respect to calcite, ACC and $SrCO_3$ are calculated as described in the Appendix and presented in Table 5.

3.2. Kinetics of calcite formation reactions

3.2.1. Initial rate of reaction (R) and order of reaction with respect to calcium ions

During the course of the experiment we determined TA by online measurement and verified that TA of the precipitation solutions are kept almost constant throughout time. Therefore, we can assume that DIC (Dissolved Inorganic Carbon) is constant and that the majority of the DIC is bicarbonate (see Table 1). As a consequence we can simplify the rate law of reactions:

$$R = K^* \cdot [Ca]^x \quad (10)$$

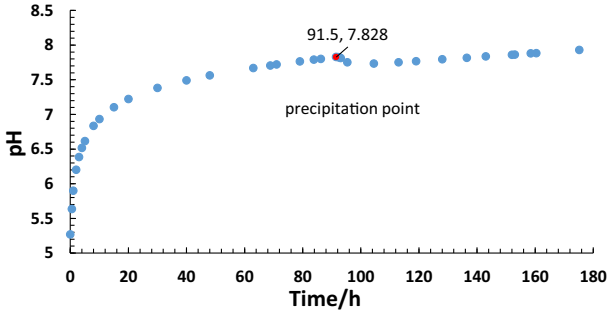

Fig. 2. The pH variations of the solution versus time of sample reaction 2 at 25 °C. The time needed to reach the saturation point is 91.5 h.

where R is the initial rate of reaction in mM/h, K^* equals the rate constant (see Eq. (11)), [Ca] is the molar concentration of Ca ions in mM and x is the order of reaction with respect to Ca ions.

$$K^* = K \cdot [HCO_3^-]^y \quad (11)$$

$[HCO_3^-]$ is the concentration of bicarbonate ions in mM and y is the order of reaction with respect to bicarbonate ions. The rate law in the previous literature, as in Zuddas and Mucci (1994), is written in the form:

$$R = k \cdot [a \cdot Ca]^x \cdot [a \cdot HCO_3^-]^y \quad (12)$$

where k is the rate constants for the forward (precipitation) reaction; a, x and y are respectively the activity and the partial reaction order of the species involved in the reaction. For simplicity we use molar concentration instead of activity.

Here we can apply the initial rate method to solve the rate law of calcite precipitation reaction following Atkins and De Paulla (2006). As an example for all reactions we plotted [Ca] versus time of randomly selected sample 38C and fitted the curve to a polynomial equation (Fig. 3a). The instantaneous rate of precipitation R is corresponding to the first derivative of the polynomial function (Eq. (13)) in Fig. 3a of data set 38C (Table 2):

$$\frac{d[Ca]}{dt} = 0.64 \cdot t - 2.59 \quad (13)$$

The first six points of sample 38C can be approximate with a linear function (Fig. 3a) according to the "initial rate method" as f.e. described by Atkins and De Paulla (2006).

$$[Ca] = -2.31 \cdot t + 10.03 \text{ and } \frac{d[Ca]}{dt} = -2.31 \quad (13a)$$

From Eq. (13a) a constant rate of −2.31 mM/h can be approximated being valid at least for the linear interval corresponding to the first six data points. For further discussion we choose the initial rate method instead of the "integration rate method" because of the closed system character of the experiment. See an extensive discussion of the use of the initial rate method in Section 3.2.4. In brief, the problem determining the "rate" is that depending on the experimental conditions we do not know when chemical equilibrium is finally reached. Based on the fact that the reaction is fast and linear in the beginning the initial rate method is a good approximation and measure of the average rate of reaction (see Fig. 3). In this regard for the first data points falling along the linear part of the curve Eq. (13a) is a good approximation for the more general curve (13). Repeating this for all experiments we make all values much more comparable and exclude the problem of reaching the chemical equilibrium. For more details see Section 3.2.4.

In order to calculate the order of reaction (x) we took the log of both sides of (Eq. (10)), we get:

$$Log\ R = \log\ K^* + x \cdot \log\ [Ca] \quad (14)$$

Plotting log R versus log [Ca] we get a linear relationship where the slope is the order of reaction (x) with respect to Ca ions as shown in (Fig. 3b). We can see that the order of reaction for the formation of $CaCO_3$ with respect to Ca ions for sample 38C is about 1.09 and hence approximately first

Table 1
Temperature (T), total alkalinity (TA), pH, salinity, concentration of ammonia [NH_3], dissolved inorganic carbon (DIC), carbonate $[CO_3]^{2-}$ and bicarbonate ions concentrations $[HCO_3]^-$, mole fraction of bicarbonate in DIC, initial and final concentrations of both [Ca] and [Sr] and their remaining fraction at the end of each experiment, Sr:Ca ratio in the mother solution ($[Sr]_0/[Ca]_0$), ratio of initial $[Ca]_0$ to the concentration of the dissolved inorganic carbon (Ca_0:DIC), time needed for each reaction to start precipitation and the period of precipitation, volume of aqueous solution, moles of $CaCO_3$ produced and its surface area.

Sample label	*T*/°C ± 0.2	[TA]/ mM	pH	Salinity	$[NH_3]$/ mM	[DIC]/ mM	$[CO_3]$/ mM	$[HCO_3]$/ mM	Mole fraction of $[HCO_3^-]$ in [DIC]	$[Ca]_0$ / mM	$[Ca]_f$ / mM	Fraction of Ca remain	[Sr]0 /mM	$[Sr]_f$ /mM	Fraction of Sr remain	$[Ca]_0$: [DCI]	$[Sr]_0/[Ca]_0$	Time needed to start precipitation/h	Time of precipitation/ h	Volume of solution / ml	Moles of $CaCO_3$	Area of $CaCO_3$/ m^2
1	**2**	**3**	**4**	**5**	**6**	**7**	**8**	**9**	**10**	**11**	**12**	**13**	**14**	**15**	**16**	**17**	**18**	**19**	**20**	**21**	**22**	**23**
20A	37.5	15.63	8.008	33.3	9.82	5.81	0.79	4.24	0.84	9.85	5.71	0.58	0.104	0.099	0.95	1.70	0.011	93.67	21.70	500	0.00207	0.122
20B	37.5	16.90	8.048	33.7	10.77	6.13	0.89	4.36	0.83	9.61	4.54	0.47	0.053	0.049	0.92	1.57	0.005	95.00	21.67	500	0.00254	0.150
21A	37.5	31.65	8.313	32.7	20.10	11.55	2.47	6.61	0.73	9.89	2.09	0.21	0.103	0.081	0.79	0.86	0.010	8.65	5.95	525	0.00410	0.242
21B	37.5	26.57	8.264	32.3	17.83	8.74	1.75	5.24	0.75	9.65	2.64	0.27	0.052	0.043	0.83	1.10	0.005	8.00	5.63	525	0.00368	0.217
22A	37.5	21.10	8.162	32.1	14.04	7.06	1.22	4.62	0.79	9.30	3.87	0.42	0.100	0.091	0.91	1.32	0.011	18.50	5.27	550	0.00298	0.176
22 B	37.5	17.10	8.112	32.2	12.44	4.66	0.75	3.17	0.81	9.30	4.25	0.46	0.050	0.046	0.92	2.00	0.005	18.50	4.10	550	0.00278	0.164
23C	37.5	30.58	8.313	32.5	20.05	10.53	2.25	6.02	0.73	9.31	1.82	0.20	0.100	0.075	0.75	0.88	0.011	5.00	3.75	550	0.00412	0.243
23D	37.5	29.11	8.310	32.3	19.85	9.27	1.98	5.31	0.73	9.31	1.62	0.17	0.050	0.037	0.74	1.00	0.005	6.00	3.75	550	0.00423	0.249
47A	37.5	17.58	8.025	31.5	10.25	7.34	1.02	5.29	0.84	9.82	3.61	0.37	0.094	0.078	0.83	1.34	0.010	6.35	1.43	400	0.00249	0.147
47B	37.5	16.12	8.019	32.3	10.07	6.04	0.83	4.38	0.84	10.12	4.80	0.47	0.049	0.043	0.88	1.68	0.005	6.73	1.25	400	0.00213	0.126
48C	37.5	67.41	8.755	30.7	55.64	11.77	3.97	3.83	0.49	9.61	4.93	0.51	0.092	0.085	0.92	0.82	0.010	3.17	0.97	400	0.00187	0.110
48D	37.5	63.20	8.716	31.6	50.92	12.28	4.02	4.24	0.51	10.12	5.69	0.56	0.049	0.045	0.92	0.82	0.005	2.85	0.97	400	0.00177	0.105
6	37.5	24.61	8.315	32.6	9.47	15.14	0.82	14.32	0.95	9.97	0.25	0.03	0.119	0.077	0.65	0.66	0.012	7.80	16.63	400	0.00389	0.229
43C	25.0	28.33	8.330	31.7	20.70	7.63	1.24	5.16	0.81	10.03	5.36	0.53	0.101	0.088	0.87	1.31	0.010	7.25	0.88	400	0.00187	0.110
43D	25.0	37.51	8.458	31.8	27.93	9.59	1.88	5.83	0.76	10.04	2.82	0.28	0.052	0.040	0.77	1.05	0.005	5.00	2.32	400	0.00289	0.171
44A	25.0	26.77	8.343	31.5	21.22	5.55	0.92	3.72	0.80	10.45	6.95	0.67	0.051	0.047	0.92	1.88	0.005	5.50	0.90	400	0.00140	0.083
44B	25.0	33.70	8.443	31.8	26.80	6.90	1.32	4.26	0.76	10.37	5.59	0.54	0.051	0.046	0.90	1.50	0.005	4.60	2.02	400	0.00191	0.113
45C	25.0	15.63	8.058	31.0	10.98	4.65	0.47	3.70	0.89	9.94	5.80	0.58	0.096	0.086	0.90	2.14	0.010	16.00	1.18	400	0.00166	0.098
45D	25.0	14.85	7.973	31.5	9.06	5.79	0.50	4.79	0.91	10.57	6.79	0.64	0.052	0.048	0.92	1.83	0.005	18.50	1.83	400	0.00151	0.089
46E	25.0	12.80	7.847	31.2	6.78	6.02	0.41	5.20	0.93	10.21	5.08	0.50	0.098	0.083	0.85	1.70	0.010	12.80	1.33	400	0.00205	0.121
46F	25.0	11.23	7.786	31.6	5.88	5.35	0.32	4.71	0.94	10.50	6.51	0.62	0.051	0.046	0.90	1.96	0.005	12.80	1.83	400	0.00160	0.094
2	25.0	12.81	7.828	31.0	8.23	4.58	0.28	4.03	0.94	9.74	2.48	0.25	0.107	0.094	0.88	2.13	0.011	91.50	83.70	400	0.00290	0.171
3	25.0	20.91	8.092	31.9	15.16	5.75	0.64	4.48	0.88	9.28	0.14	0.02	0.107	0.068	0.64	1.61	0.012	7.13	50.80	400	0.00366	0.216
4	25.0	8.58	7.654	33.0	5.50	3.08	0.15	2.79	0.95	19.84	7.96	0.40	0.108	0.095	0.88	6.44	0.005	9.05	14.25	400	0.00475	0.280
7	25.0	4.64	7.753	48.0	3.64	1.00	0.04	0.92	0.96	149.00	143.80	0.97	0.000	n.d.	n.d	149.00	n.d.	3.40	3.00	400	0.00208	0.122
8	25.0	2.46	7.383	48.0	1.34	1.10	0.02	1.06	0.98	148.42	139.73	0.94	1.510	1.480	0.98	134.93	0.010	3.40	3.10	400	0.00348	0.205
37A	12.5	18.46	8.020	32.0	10.15	8.31	0.52	7.27	0.93	10.05	2.39	0.24	0.101	0.076	0.75	1.21	0.010	10.25	3.55	400	0.00306	0.181
37B	12.5	16.70	7.993	31.8	9.52	7.19	0.42	6.34	0.94	9.93	3.32	0.33	0.051	0.040	0.78	1.38	0.005	11.70	2.12	400	0.00264	0.156
38C	12.5	11.53	7.839	31.7	6.64	4.89	0.21	4.47	0.96	10.05	4.65	0.46	0.101	0.089	0.88	2.06	0.010	14.00	4.38	400	0.00216	0.127
38D	12.5	18.46	8.084	31.9	11.72	6.74	0.48	5.79	0.92	10.00	3.06	0.31	0.051	0.041	0.80	1.48	0.005	12.50	5.17	400	0.00278	0.164
39A	12.5	14.16	8.019	31.8	10.03	4.14	0.26	3.62	0.93	9.97	7.84	0.79	0.101	0.099	0.98	2.41	0.010	84.00	4.07	400	0.00085	0.050
39B	12.5	14.07	8.008	31.8	9.78	4.29	0.26	3.77	0.94	9.96	7.30	0.73	0.052	0.050	0.96	2.32	0.005	76.00	5.00	400	0.00106	0.063
40C	12.5	11.43	7.767	31.8	5.64	5.79	0.21	5.37	0.96	9.91	5.28	0.53	0.101	0.090	0.89	1.71	0.010	19.00	3.25	400	0.00185	0.109
41E	12.5	16.12	8.048	31.7	10.75	5.37	0.35	4.66	0.93	9.94	5.46	0.55	0.102	0.089	0.87	1.85	0.010	15.37	2.50	400	0.00179	0.106
41F	12.5	15.14	7.986	31.8	9.33	5.81	0.34	5.13	0.94	10.06	4.85	0.48	0.052	0.046	0.88	1.73	0.005	21.75	3.38	400	0.00208	0.123
42A	12.5	20.42	8.181	31.5	14.62	5.80	0.50	4.80	0.91	9.84	5.29	0.54	0.103	0.089	0.86	1.70	0.010	15.00	2.95	400	0.00182	0.108
42B	12.5	17.88	8.099	31.7	12.10	5.77	0.42	4.93	0.92	9.88	6.19	0.63	0.052	0.046	0.88	1.71	0.005	24.75	2.38	400	0.00148	0.087

Notes: n.d. = not detected. TA was measured from titrating the final solution with HCl, pH and salinity were measured at the end of each reaction. [NH_3], $[CO_3^{2-}]$, [DIC] and $[HCO_3^-]$ were calculated from Eqs. a2, a4 and a1 as seen in the Appendix, respectively. Mole fraction of HCO_3^- (**column10**) = column **9** /(column **9** + column **8**). Initial and final concentration of Ca and Sr (columns **11**, **12**, **14** and **15**) are measured by ICP-MS. **Column13** = column **12** /column **11**. **Column16** = column **15** /column **14**. **Column17** = column **11**/column **7**. **Column18** = column **14**/column **11**. **Column 22 =** [(column **11** − column **12**) * column **21**] * 10^{-6}. **Column 23 =** column **22** × 59 m^2/mol.

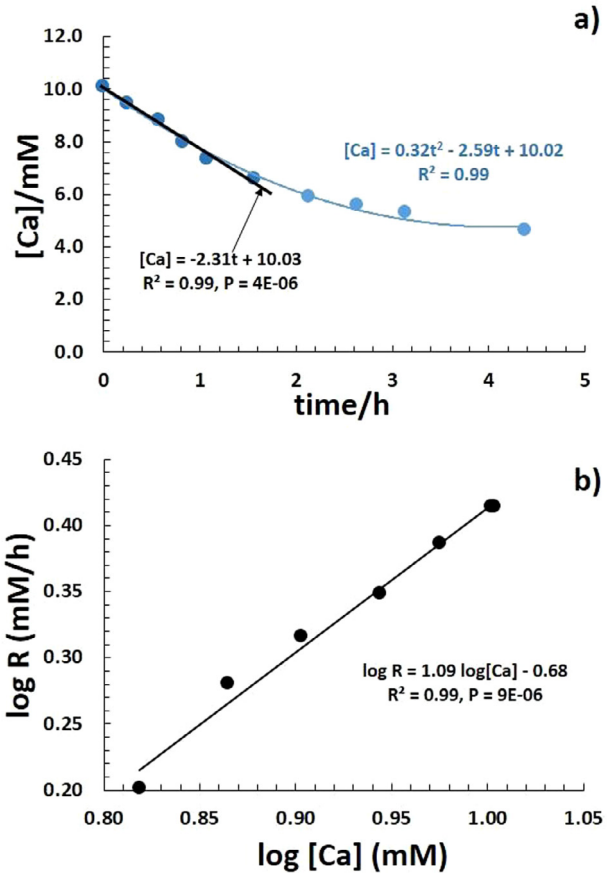

Fig. 3. Example for the kinetics of calcite formation reaction. (a) Changes of Ca^{2+}-ion concentration as function of time for arbitrarily selected sample reaction 38C to produce calcite at 12.5 °C. Latter values fit a quadratic polynomial function. The instantaneous rate of reaction corresponds to the first derivative of the polynomial equation. The linear approximation of the first samples of the curve equals the initial rate of reaction. (b) Plotting log instantaneous rate as a function of log [Ca]. The slope of this linear relationship equals to the order of reaction with respect to Ca ions.

order. We repeated these calculations for all reactions (Table 5) at all temperatures. These calculations show that all measurements range from 0.77 to 1.26 for the order or reaction (x) with an average value of 1.02 ± 0.17 (1 SD). Hence, we report the order of reaction with respect to [Ca] to be one. However, applying the average value of one to one specific experiment will reproduce inconsistent results when not taking the standard deviation of the order of reaction into account. Note that our results are in general accord with in the literature as f.e. in Kazmierczak et al. (1982).

3.2.2. Order of reaction with respect to bicarbonate ions

For simplicity we assume that DIC $\sim [HCO_3^-]$ because the majority of DIC are bicarbonate ions (see Table 1 column 10). In this case we can write:

$$R = k \cdot [Ca]^1 \cdot [HCO_3^-]^y \quad (15)$$

At time zero for most of reactions (Eq. (15)) can be written as:

$$R = 10 \cdot k \cdot [HCO_3^-]^y \quad (16)$$

taking logarithm of both sides of (Eq. (16)) we get:

$$Log\ R = \log 10 \cdot k + y \cdot \log\ [HCO_3^-] \quad (17)$$

There is a relatively large individual variation in the k value from one experiment to the other. Taking the k value from one single experiment only is not sufficient because it is burdened with large uncertainties. For example for all 12.5 °C experiments the k value varies from 0.00043 to 0.00142 with an average value of 0.0008 ± 0.0003 corresponding to an uncertainty of about 40%. Latter value can also be calculated from Eq. (10) and from the graphic extrapolation of Eq. (17) as seen from (Fig. 4).

From a fit of our three calculated rate constants (for 12.5 °C, 25 °C, 37.5 °C) we fit the Arrhenius equation and from the slope calculated to be ~−13,756 and estimate the activation energy (E_a) for the calcite formation to be ~114 kJ/mol. Latter value is in general agreement with literature data as reported by Kazmierczak et al. (1982), Nancollas and Reddy (1971) and Wiechers et al. (1975) who estimated E_a of calcite growth in the range of 40–50 kJ/mol, while Koutsoukos and Kontoyannis (1984) estimated E_a in the absence of seed crystals to be 155 kJ/mol. The slight discrepancy between data is attributed to different experimental setups. However, the general agreement of our calculated data with those from earlier experiments support our experimental approach presented here.

Table 2
Data of reaction 38C to produce calcite at 12.5 °C.

Sample:	[Ca]/ppm	± 2 SD of the mean	Time/h ± 0.008	[Ca]/mM	± 2 SD of the mean	Instantaneous rate mM/h	log [Ca]	log Rate
C0	404	3	0	10.08	0.08	2.59	1.004	0.41
C1	379	2	0.25	9.45	0.05	2.43	0.975	0.39
C2	353	0	0.57	8.80	0.01	2.23	0.944	0.35
C3	320	1	0.82	8.00	0.04	2.07	0.903	0.32
C4	294	3	1.07	7.33	0.07	1.91	0.865	0.28
C5	264	2	1.57	6.59	0.04	1.59	0.819	0.20
C6	236	1	2.13	5.90	0.03			
C7	224	1	2.63	5.59	0.03			
C8	213	1	3.13	5.30	0.02			
Cf	187	2	4.38	4.65	0.04			

Note: Instantaneous rate is calculated by substituting time in Eq. (13).

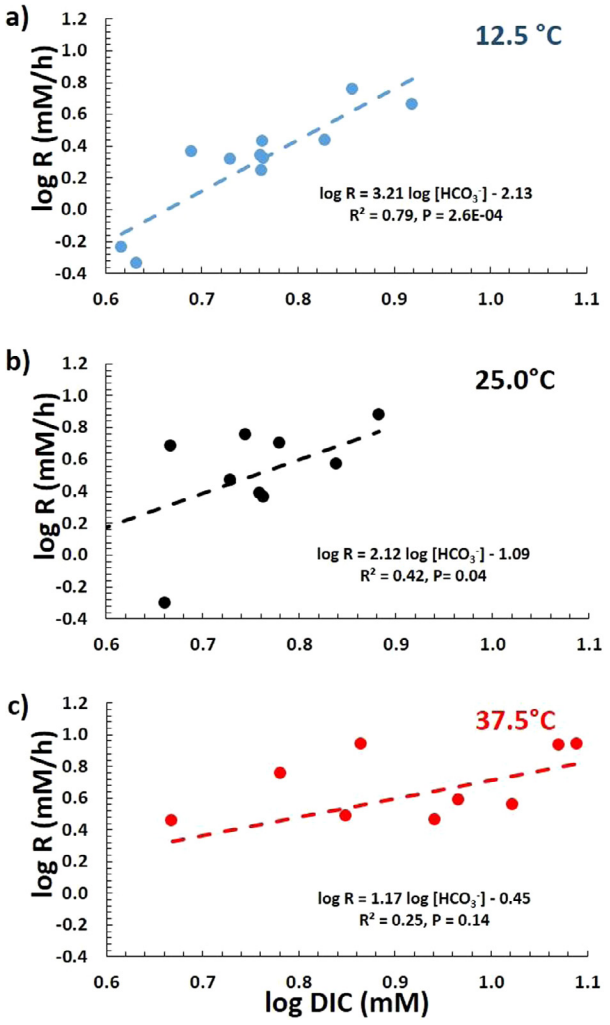

Fig. 4. Log initial rate versus log DIC at (a) 12.5, (b) 25.0 and (c) 37.5 °C. The slopes of these curves equal the orders of reaction with respect to bicarbonate ions and y-intercept equals log (10 * rate constant).

Table 3
Order of reactions with respect to HCO_3^- ions and the rate constant at three different temperatures.

Temperature, °C	Order of reaction with respect to HCO_3^-	Rate content $mM^{-x} \cdot h^{-1}$
1	**2**	**3**
12.5	3	7.38×10^{-4}
25.0	2	80.6×10^{-4}
37.5	1	352×10^{-4}

Note: Values of this table are obtained from Fig. 4. **Column 2:** rounded to the closest integer. **Column 3**: obtained from the y-intercept of Eq. (17). × = values in Column 2.

If we plot log R versus log [DIC] then the slope of this relationship is y, the order of reaction with respect to bicarbonate ions and its y-intercept equals to log 10 k, as shown in (Fig. 4) and summarized in Table 3. The order of reaction with respect to $[HCO_3^-]$ is changing with temperature from around one (37.5 °C), to around two (25 °C) and three (12.5 °C) which means that the mechanism of calcite formation depend on the experimental conditions as reported earlier in Burton and Walter (1987), Zuddas and Mucci (1998), Lopez et al. (2009) and Zuddas and Mucci (1994). Literature values of the order of reaction "y" with respect to carbonate ions are summarized in Table 4. There it can be seen by raising temperature from 12.5 to 25 °C results in an about 11 fold increase in the rate constant value. While raising temperature from 25 to 37.5 °C results in an about 4.4 fold increase in the rate constant value as reported for most of the noncomplex chemical reactions as also reported in Atkins and De Paulla (2006).

3.2.3. Crystalline structure and rate of reactions normalized to the average specific surface area (R^*)

The X-ray diffraction spectra show that more than 95% of the signal intensity refers to calcite. The residual of less than 5% of the signal is a contribution of unspecified background noise. In this regard, the abundance of strontianite ($SrCO_3$) in significant quantities in any of the solid samples cannot be confirmed.

The SEM images as seen in (Fig. 5a) indicate that all calcite crystals of our experiments show the typical rhombohedra micro-morphology. We utilized secondary electron (SE) images from SEM to estimate the average specific surface area of calcite obtained from different experiments since the quantity of calcite products were insufficient for BET-determination (BET = Brunauer–Emmett–Teller) of the surface area. In order to calculate the specific rate of precipitation (R^*) we determined the surface area and the volume of 50 randomly selected calcite crystals from 10 samples which differ in R^* and temperature (Fig. 5b). For the randomly selected crystals the dimension of the length, width and height are measured individually from which than the surface area as well as the volume has been calculated. Then the average value of all individual surface areas and volumes are taken. From this the specific surface area S was calculated according to:

$$S = \frac{\text{total area}(\mu m^2)}{[\text{total volume}\ (\mu m^3) \times \text{density of calcite}\ (2.71.10^{-12}\ g\mu m^{-3})]} \quad (18)$$

The results corresponds to an average value for S of 0.59 m^2/g. In order to verify the S values for temperature dependency ten different calcite samples precipitated at different rate and temperature are measured and calculated in the same way (Fig. 5b). It can be seen from Fig. 5b that the S values are independent of temperature and the initial rate of reaction. As a consequence we assume that S is constant for all calcite precipitates and that an average values of 0.59 m^2/g or equivalent to 59.0 m^2/mol can be adopted. Values of normalized rate of precipitation R^* ($\mu mol/m^2 \cdot h$) are summarized in Table 5 and are calculated from:

$$R^* = \frac{\text{initial rate}(mM/h) \times \text{volume of reacting solution}(ml)}{\text{Area of CaCO}\ (m^2)} \quad (19)$$

where the value of the numerator equals the initial rate ($\mu mol/h$), the total area of $CaCO_3$ in each sample reaction

Table 4
Literature values concerning the order of reaction of carbonate ions in calcite precipitation as function of experimental conditions.

Literature value	Order of reaction with respect to CO_3^{2-} ions	Order of reaction with respect to HCO_3^- ions	Experimental condition
Burton and Walter (1987)	0.6–2.3		Temperature changes from 5 to 37 °C
Zuddas and Mucci (1998)	1–3		Ionic strength changes from 0.10 to 0.93 molal
Lopez et al. (2009)	2–5		Temperature changes from 5 to 70 °C
Zuddas and Mucci (1994)		2	At 25 °C

equals the moles of $CaCO_3$ produced at the end of each experiment multiplied by S.

3.2.4. Calculation of rate and the order of reaction with respect to the "Initial Rate Method" versus the Lemarchand et al. (2004) estimation of rate

One of the most important parameters in chemical precipitation experiments is the rate law (R) and the specific precipitation rate (R^*). There are several methods known in the literature to determine R^* depending on the individual experimental setup like the initial rate method (this study), the integration rate method (Atkins and De Paulla (2006)) and the average rate method (c.f. Tang et al. (2008)).

Depending on the experimental conditions when [Ca] decreases fast, the linear relationship at the beginning of the experiment deviates from linearity with time. Hence, the problem then is to estimate a representative R^* for the whole experiment. From the three methods mentioned above we choose the "initial rate method" for our closed system approach. Although laborious it is straight forward, neither assumption have to be made and nor constants have to be known in advance. The "initial rate method" is used here as a first order approximation of the average rate law within a certain time interval from the beginning of the precipitation experiment (t_0) to a certain time (t_1) at which the drop of [Ca] is linear. For example in Fig. 3 it can be seen that the values of randomly selected sample 38C can be approximated by a linear curve for about one third of the total experimental time. This time interval also corresponds to about 65% of the initial [Ca] precipitated for sample 38C. In Table 5 column 5 we have summarized the amount of material precipitated and corresponding to the linear part of the precipitation curve. The values vary between 33 and ~100%. In average about 80% of the total amount of Ca precipitated under linear conditions. Although the majority of the material precipitated under linear conditions and taken in this study to represent the whole experiment we clearly note that strictly speaking the approximation of a linear precipitation rate is only valid for the linear part of the precipitation curve as shown for example in Fig. 3a and do not necessarily account for the non-linear part of the precipitation curve in the second part of the curve.

It may also be argued that the initial rate method is not adequate to describe reversible processes where precipitation and dissolution processes are involved as well as kinetic and equilibrium fractionation processes may occur simultaneously. However, as shown in the Appendix calculation of the fractionation factor α calculated from values taken from the non-linear part fit the experimental data quite well (see Appendix). This may imply that the α value of the linear and non-linear part do not deviate to a large extend. In contrast to our approach to calculate R^*, Lemarchand et al. (2004) used Eq. (20) in their experimental system to estimate R^*(μmol/m^2·h), where the values for "n_2" and "k_f" are calculated for seawater and seawater like systems from Zuddas and Mucci (1994). For NaCl-$CaCl_2$ solutions at 25 °C corresponding to ionic strength, I = 0.55 and I = 0.93 ($n_2 = 3.34$, log $k_f = 6.24$ and $n_2 = 2.73$, log $k_f = 6.07$, respectively) and $[CO_3^{2-}]$ is in mM.

$$LogR^* = \log k_f + n_2 \cdot \log([CO_3]^{2-}), \tag{20}$$

where "k_f" is the rate constant "n_2" refers to the order of reaction

In Fig. B and Table C of the Appendix we compare our measured R^* values with those calculated using the Lemarchand et al. (2004) approach and the related constants.

As it can be seen there is no relationship between the measured and estimated R^* values which are except for two values tend to be significantly lower than the measured ones. From Fig. B it can be seen that the precipitation rates calculated following the Lemarchand approach and our approach greatly deviate from the 1:1 line. Except for two values the Lemarchand et al. rates tend to be significantly lower than those measured in this study. We attribute these differences to the fact that the precipitation rates calculated by Lemarchand et al. are mainly based on assumption and constants only valid for seawater but not for solutions containing larger concentrations on ammonia. Hence, for further discussions we consider our approach and the measured R^* value to be the best approach to estimate calcite precipitation rates.

3.3. Strontium incorporation into calcite

In a closed system Sr incorporation into calcite can be described by Usdowski (1975) as:

$$\left(\frac{[Sr]}{[Ca]}\right)_{calcite} = \left(\frac{[Sr]}{[Ca]}\right)_{aq,0} \cdot \frac{\left(1 - \left[\left(\frac{[Ca]}{[Ca]}\right)_0\right]^{D_{Sr}}\right)}{\left(1 - \left[\left(\frac{[Ca]}{[Ca]}\right)_0\right]_{aq}\right)} \tag{21}$$

where $([Sr]/[Ca])_{calcite}$ is the molar ratio of the calcite, $([Sr]/[Ca])_{aq,0}$ is the molar ratio of these ions in the solution, $([Ca]/[Ca]_0)$ is the fraction of Ca that remains in aqueous solution at any time and D_{Sr} is the distribution constant of Sr between solution and the calcite ($([Sr]/[Ca])_{calcite}/([Sr]/[Ca])_{aq}$). We validate this equation to our system of

Table 5
Initial rate, rate normalized to surface area (R^*), log R^*, saturation index (SI) with respect to [amorphous $CaCO_3$ (ACC), calcite and $SrCO_3$], strontium distribution constant (D_{Sr}), log D_{Sr}, $\Delta^{88/86}Sr$ (‰) uncorrected and corrected values, $\Delta^{44/40}Ca$ (‰) uncorrected and corrected values.

Sample label	Initial rate/ mM/h	Normalized rate (R^*)/ μmol/m^2·h	log R^*	[Ca] consumed (%)	SI. ACC	SI. calcite	SI. $SrCO_3$	D_{Sr}	±(2SEM)	Log D_{Sr}	±(2SEM)	$\Delta^{88/86}Sr$ (‰) uncorrected	$\Delta^{88/86}Sr$ (‰) corrected	±(2SEM)	$\Delta^{44/4\circ}Ca$ (‰) uncorrected	$\Delta^{44/4\circ}Ca$ (‰) corrected	±(2SEM)
1	**2**	**3**	**4**	**5**	**6**	**7**	**8**	**9**	**10**	**11**	**12**	**13**	**14**	**15**	**16**	**17**	**18**
20A	0.30	1230	3.09	93	1.10	1.32	2.22	0.099	0.003	−1.003	0.014	−0.173	−0.177	0.004			
20B	0.79	2640	3.42	71	1.14	1.36	1.98	0.078	0.002	−1.107	0.011	−0.145	−0.150	0.016	−0.49	−0.73	0.19
21A	3.17	6890	3.84	82	1.60	1.82	2.71	0.150	0.001	−0.824	0.003	−0.163	−0.184	0.007			
21B	2.90	7010	3.85	88	1.44	1.66	2.26	0.130	0.002	−0.886	0.005	−0.177	−0.195	0.007			
22A	3.06	9560	3.98	66	1.26	1.48	2.39	0.124	0.003	−0.906	0.012	−0.202	−0.212	0.011			
22B	2.84	9530	3.98	87	1.05	1.27	1.88	0.122	0.002	−0.912	0.006	−0.198	−0.208	0.004	−0.82	−1.24	0.09
23C	3.61	8170	3.91	95	1.53	1.75	2.65	0.164	0.003	−0.785	0.009	−0.199	−0.230	0.002	−0.41	−1.04	0.15
23D	3.85	8490	3.93	73	1.48	1.70	2.30	0.153	0.003	−0.816	0.010	−0.231	−0.270	0.004	−0.73	−1.97	0.10
47A	8.65	23,580	4.37	94	1.21	1.43	2.28	0.189	0.003	−0.723	0.008	−0.242	−0.267	0.014			
47B	5.66	18,030	4.26	87	1.13	1.35	1.91	0.192	0.007	−0.717	0.016	−0.233	−0.249	0.005	−1.07	−1.59	0.13
48C	8.62	31,220	4.49	92	1.79	2.01	2.87	0.191	0.004	−0.719	0.009	−0.253	−0.264	0.013			
48D	8.69	33,210	4.52	67	1.82	2.04	2.60	0.179	0.008	−0.748	0.020	−0.232	−0.242	0.006	−1.14	−1.54	0.24
6	2.54	4430	3.65	74	1.12	1.34	2.29	0.096	0.002	−1.016	0.009	−0.137	−0.172	0.010			
43C	7.54	27,360	4.44	54	1.14	1.52	2.37	0.215	0.005	−0.668	0.009	−0.275	−0.296	0.008	−0.93	−1.29	0.15
43D	4.26	9990	4.00	64	1.32	1.70	2.26	0.203	0.007	−0.692	0.015	−0.257	−0.294	0.007			
44A	5.68	27,510	4.44	75	1.02	1.41	1.94	0.202	0.001	−0.695	0.000	−0.292	−0.304	0.008	−1.06	−1.31	0.10
44B	3.70	13,120	4.12	81	1.18	1.56	2.10	0.212	0.004	−0.674	0.009	−0.276	−0.292	0.001	−1.03	−1.42	0.10
45C	4.82	19,720	4.30	81	0.71	1.10	1.93	0.219	0.006	−0.659	0.012	−0.297	−0.313	0.017			
45D	2.30	10,320	4.01	84	0.76	1.15	1.69	0.194	0.003	−0.712	0.007	−0.250	−0.260	0.005	−1.33	−1.67	0.15
46E	5.01	16,550	4.22	74	0.66	1.05	1.87	0.224	0.003	−0.65	0.006	−0.283	−0.307	0.014			
46F	2.94	12,490	4.10	90	0.57	0.95	1.48	0.243	0.007	−0.615	0.012	−0.282	−0.300	0.012	−1.22	−1.57	0.10
2	0.50	1170	3.07	71	0.48	0.86	1.75	0.059	0.001	−1.231	0.010	−0.111	−0.118	0.009	−0.54	−1.16	0.10
3	2.44	4520	3.66	73	0.82	1.20	2.11	0.113	0.002	−0.949	0.007	−0.123	−0.156	0.005			
4	1.10	1570	3.20	33	0.52	0.88	1.48	0.103	0.002	−0.987	0.008	−0.203	−0.217	0.003			
7	3.19	10,471	4.02	97	0.82	1.20									−1.52	−1.55	0.15
8	3.65	7120	3.85	84	0.51	1.15	1.75	0.174	0.004	−0.76	0.010	−0.231	−0.233	0.003			
37A	4.56	10,090	4.00	65	0.58	1.13	2.00	0.198	0.006	−0.703	0.012	−0.272	−0.314	0.018	−0.58	−1.29	0.11
37B	5.72	14,660	4.17	89	0.48	1.03	1.61	0.218	0.004	−0.661	0.009	−0.305	−0.347	0.007	−0.79	−1.43	0.18
38C	2.31	7250	3.70	65	0.18	0.74	1.61	0.163	0.005	−0.789	0.013	−0.254	−0.271	0.004			
38D	2.71	6620	3.82	78	0.54	1.10	1.67	0.184	0.003	−0.735	0.007	−0.267	−0.301	0.003	−0.79	−1.51	0.09
39A	0.58	4630	3.67	75	0.27	0.83	1.70	0.178	0.009	−0.751	0.021	−0.260	−0.263	0.012	−1.52	−1.71	0.17
39B	0.46	2940	3.47	80	0.27	0.83	1.41	0.165	0.006	−0.782	0.017	−0.234	−0.239	0.007			
40C	1.75	6410	3.81	83	0.18	0.73	1.61	0.203	0.007	−0.693	0.014	−0.252	−0.267	0.007	−1.15	−1.60	0.16
41E	2.08	7870	3.90	100	0.40	0.95	1.83	0.201	0.006	−0.698	0.012	−0.278	−0.299	0.005	−1.24	−1.70	0.12
41F	2.1	6840	3.84	93	0.39	0.95	1.53	0.194	0.004	−0.712	0.010	−0.260	−0.277	0.006			
42A	2.67	9930	4.00	89	0.55	1.11	1.99	0.198	0.005	−0.704	0.010	−0.275	−0.295	0.006			
42B	2.19	10,050	4.00	94	0.48	1.03	1.62	0.225	0.005	−0.648	0.009	−0.285	−0.301	0.005			

Note: For all reactions the initial rate (mM/h) was calculated according to the initial rate law (see text). The precipitation rate R^* is calculated according to Eq. (19) in the text. The saturation index SI of different minerals (columns 6, 7 and 8) are calculated as reported in the Appendix. **Column 5:** this column shows the amount of Ca (%) corresponding to the linear decreasing part of [Ca]. In average about 80% of the precipitated Ca corresponds to the linear part. The D_{Sr} values are calculated from Eq. (21). **Columns 13** and **16**: these columns show the measured isotope values of Sr and Ca respectively, uncorrected for the reservoir effect. **Columns 14** and **17**: are the corrected values of columns **13** and **16** respectively using Eqs. (7) and (8) in the text.

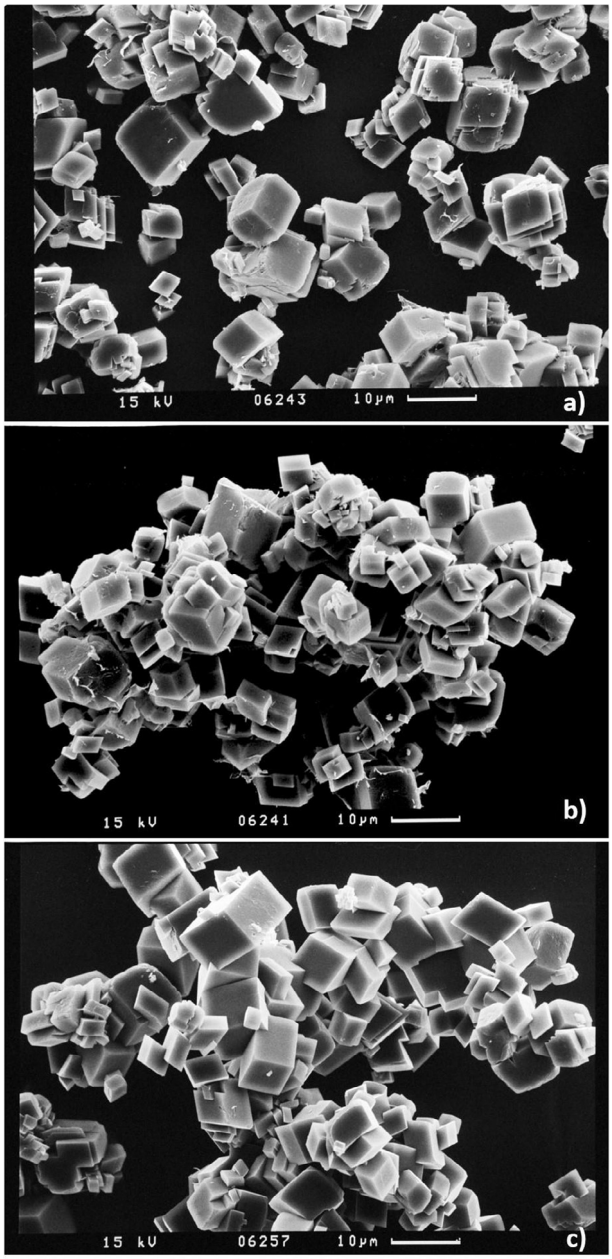

Fig. 5a. SEM images of some calcite crystals, (a) T= 12.5 °C of sample reaction 37B; (b) T= 25.0 °C, of sample reaction 43C and (c) T= 37.5 °C of sample reaction 48D.

precipitation reactions as in Tang et al. (2008a) by plotting $\log\{([Sr]/[Ca]_{aq}/([Sr]/[Ca])_{aq,0}\}$ versus $\log([Ca]_{aq}/[Ca])_{aq,0})$. The slope of this relationship equals $D_{Sr} - 1$ (see Fig C in the Appendix and Table 5 for more details).

From Fig. 6a–c for all temperatures as R^* increases more Sr will be incorporated into calcite and D_{Sr} increases. There is one critical observation in the 25 °C data set (Fig. 6b) for the lowest R^* values where it seems that D_{Sr} may depend on the initial $(Sr/Ca)_0$ values. However, for the other data sets no such behavior can be recognized but cannot completely be excluded for R^* values not covered by our study.

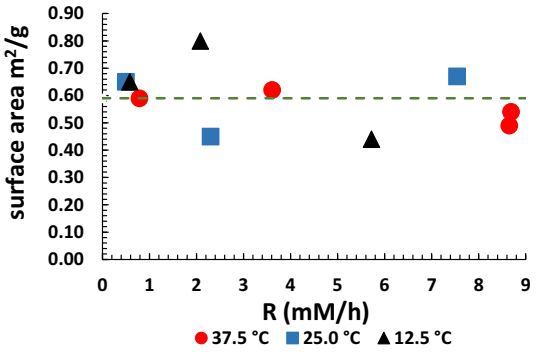

Fig. 5b. Specific surface area of arbitrarily selected 10 samples of calcite at different rate and temperature, calculated as described in the text. The dashed line represents the average surface area.

Except for the 12.5 °C data set it can be seen that at 25 and 37.5 °C the values apparently reach kind of plateaus for low and high values of R^*. For low R^* this plateau may reflect the chemical equilibrium corresponding to a zero net growth (marked as D_{Sreq}). Whereas at higher R^* the D_{Sr} may approach a distinct D_{Sr} value reflecting relatively high R^* values without any significant change of D_{Sr} (marked as D_{SrF}). Although not well defined there is a tendency of decreasing D_{Sr} with increasing temperatures in particular for lower growth rates below about 3.5 µmol/m^2·h (Fig. 6c).

3.4. Isotope analysis

3.4.1. Results of Sr isotope fractionation measurements

The $\delta^{88/86}Sr$ value of the solution was measured to be $0.175 \pm 0.002‰$ ($n = 4$). For all temperatures (Table 5, Fig. 7) as rate of precipitation increase more lighter Sr isotopes will be incorporated into calcite corresponding to decreasing $\Delta^{88/86}Sr_{calcite-aq}$ values. In contrast, as temperature increases the isotope difference to the mother solution decreases and isotope fractionation $\delta^{88/86}Sr$ values increases at the same R^*. It is interesting to note that the Sr trace element partitioning and isotope fractionation in calcite resemble each other indicating that there is an inverse linear correlation between D_{Sr} and $\Delta^{88/86}Sr$ (Fig. 8). Relationships for the different temperatures are:

$$12.5°C: \Delta^{88/86}Sr = -(1.14 \pm 0.74) \cdot D_{Sr} - (0.07 \pm 0.08); \quad R^2 = 0.61,\ p = 0.008 \tag{22}$$

$$25.0°C \text{ and } [Sr]/[Ca]_o = 0.01: \quad \Delta^{88/86}Sr = -(1.22 \pm 0.24) \cdot D_{Sr} - (0.033 \pm 0.044); \quad R^2 = 0.98,\ p = 0.0002 \tag{23}$$

$$25.0°C \text{ and } [Sr]/[Ca]_o = 0.005: \quad \Delta^{88/86}Sr = -(0.65 \pm 0.41) \cdot D_{Sr} - (0.152 \pm 0.081); \quad R^2 = 0.83,\ p = 0.01 \tag{24}$$

$$37.5°C: \Delta^{88/86}Sr = -(0.91 \pm 0.32) \cdot D_{Sr} - (0.086 \pm 0.048); R^2 = 0.78,\ p = 6 \cdot 10^{-5} \tag{25}$$

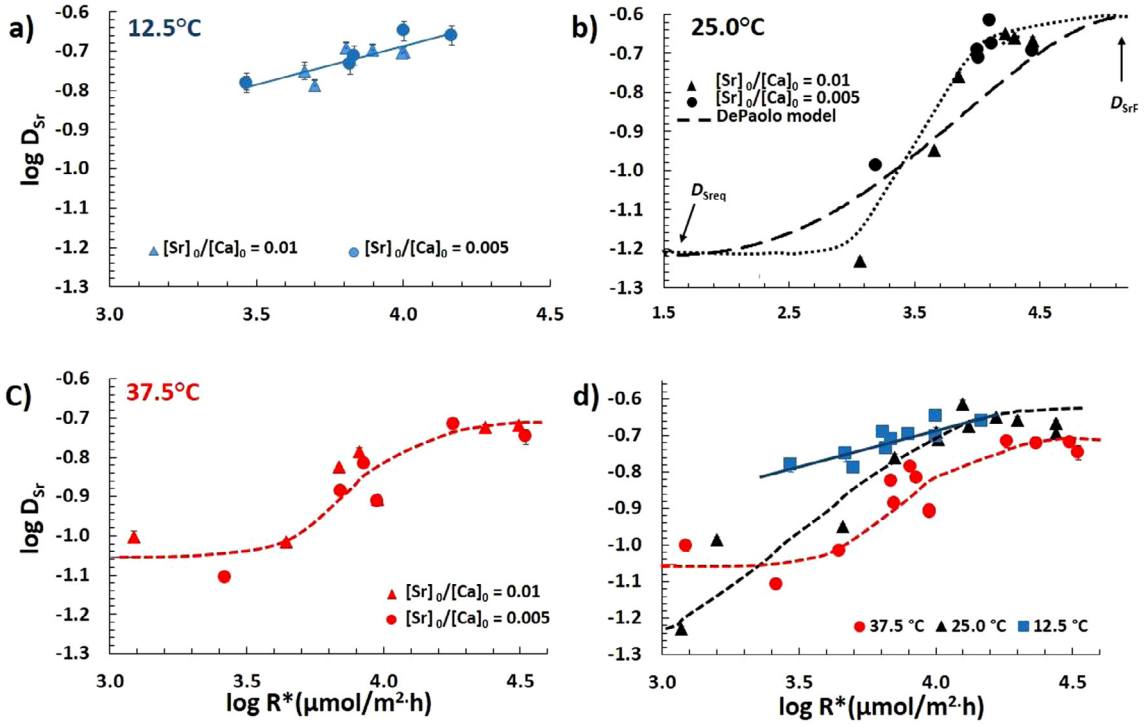

Fig. 6. Log D_{Sr} are plotted as a function of log R^* (µmol/m^2·h) of calcite precipitated at (a) 12.5 °C, (b) at 25.0 °C. In addition our results are compared with the DePaolo (2011) model which is presented as dashed line curve, (c) 37.5 °C. Note, for all temperatures two different solutions have been measured (Sr/Ca ratios of 0.01 and 0.005) in order to verify the influence of different chemical compositions on the results. d) summarizes the results of the three experiments showing that there effect of temperature and precipitation rate are different. Temperature sets the initial value and rate is modifying the initial ratio following distinct rate dependent functions.

The confidence intervals in the above expressions were calculated at a 95% confidence level. Fig. 8 shows our results are in good agreement with results of inorganic precipitated calcite of Böhm et al. (2012) who reported:

$$25.0^{\circ}C \text{ and } [Sr]/[Ca]_o = 0.01$$
$$\Delta^{88/86}Sr = -(1.5 \pm 0.7) \cdot D_{Sr} - (0.03 \pm 0.09);$$
$$R^2 = 0.89,\ p = 0.002 \quad (26)$$

Fig. 8 shows that this linear correlation between D_{Sr} and $\Delta^{88/86}Sr$ depends only on R^* but is completely independent of precipitation conditions (temperature and origin either biogenic or inorganic calcite), since all curves are overlapping with each other. The linear correlation between D_{Sr} and $\Delta^{88/86}Sr$ for all data points in Fig. 8 is presented by the solid line in the figure, it has the following general equation:

$$\Delta^{88/86}Sr = -(1.21 \pm 0.12) \cdot D_{Sr} - (0.047 \pm 0.019);$$
$$R^2 = 0.89,\ p = 1.6510^{-25} \quad (27)$$

It is noteworthy to emphasize that the $D_{Sr} - \Delta^{88/86}Sr_{calcite-aq}$ relationship depend only on R^* and hence mainly on [Ca] and $[HCO_3^-]$, respectively. However, in contrast to [Ca] which rate of reaction is one the order of reaction for $[HCO_3^-]$ varies from 1 to 3 as a function of temperature from 12.5 to 37.5 °C, respectively. Hence, in particular for relatively cooler temperatures of 12.5 and 25 °C the influence of $[HCO_3^-]$ is larger relative to [Ca] than for higher temperatures. As an example the inspection of sample 4 and 2 shows that the Ca concentration is relatively high (see Table 1, column 11, 4: [Ca] = 19.84, 2: [Ca] = 9.74 mM at 25.0 °C), nevertheless R^* is relatively low (see Table 5, column 4, 4: log $R^* = 3.20$, 2: log $R^* = 3.07$). Concerning the [DIC] the situation is different and the two samples show the lowest concentrations of 2:3.08 mM and 4.58 mM, respectively (see Table 1, column 7). The order of reaction for HCO_3^- at 25 °C is two in contrast to one for Ca which means that the effect of [DIC] on R^* is much larger than the one of [Ca]. Hence, one can expect these samples to have lower R^* values related to relatively low D_{Sr} but relatively high $\Delta^{88/86}Sr_{calcite-aq}$ values as seen from Table 5. Furthermore, looking at sample 3 it shows a relatively low [DIC] value of 5.75 mM and the lowest [Ca] at 25 °C = 9.28 mM. However, due to the fact that at 25 °C the order of reaction is 2 R^* shows a moderate value of (log R^*=3.66) among the data points in Table 5.

3.4.2. Calcium isotope analysis

The results of the Ca isotope analysis are presented in Fig. 9 and in Table 5, respectively. At 12.5 and 25.0 °C as rate of precipitation increase more heavier Ca isotopes will become incorporated into calcite which means that $\Delta^{44/40}Ca_{calcite-aq}$ values increase as a function of rate (Fig. 9a,b). However at 37.5 °C as rate of precipitation increase the $\Delta^{44/40}Ca_{calcite-aq}$ decrease. Observations at 12.5 and 25.0 °C are in general accord with the earlier observa-

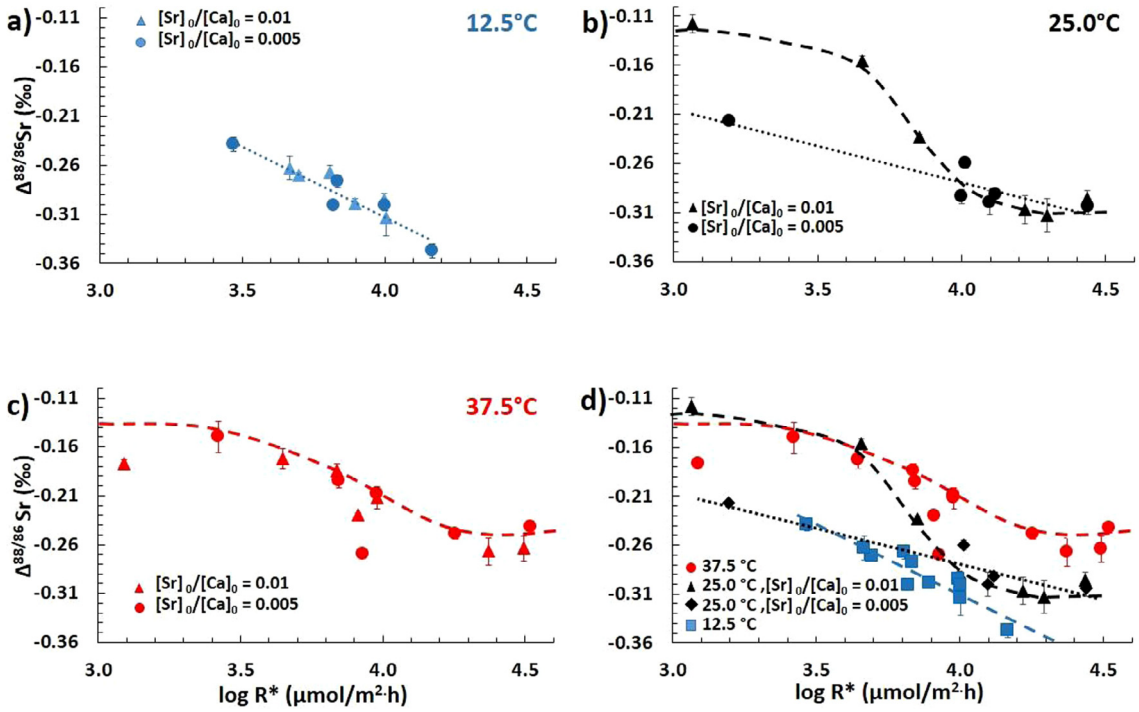

Fig. 7. This diagram shows all $\Delta^{88/86}Sr_{calcite\text{-}aq}$ values as a function of their corresponding log R^*(µmol/m^2·h) data. For all temperatures, as rate of reaction increases $\Delta^{88/86}Sr$ become more negative. Data approach plateaus at low and high rates as seen for the reaction at 25 and 37.5 °C (b and c) respectively). At 25 °C (b) above ~3.6 µmol/m^2·h the effect of the Sr/Ca ratio in the mother solution is insignificant. However, below ~3.6 µmol/m^2·h the 0.005 ratio solution tend to approach a lower equilibrium. Fig. (d) summarizes the data emphasizing the role of temperature showing that at constant R^* initial $\Delta^{88/86}Sr_{calcite\text{-}aq}$ increase as a function of increasing temperature.

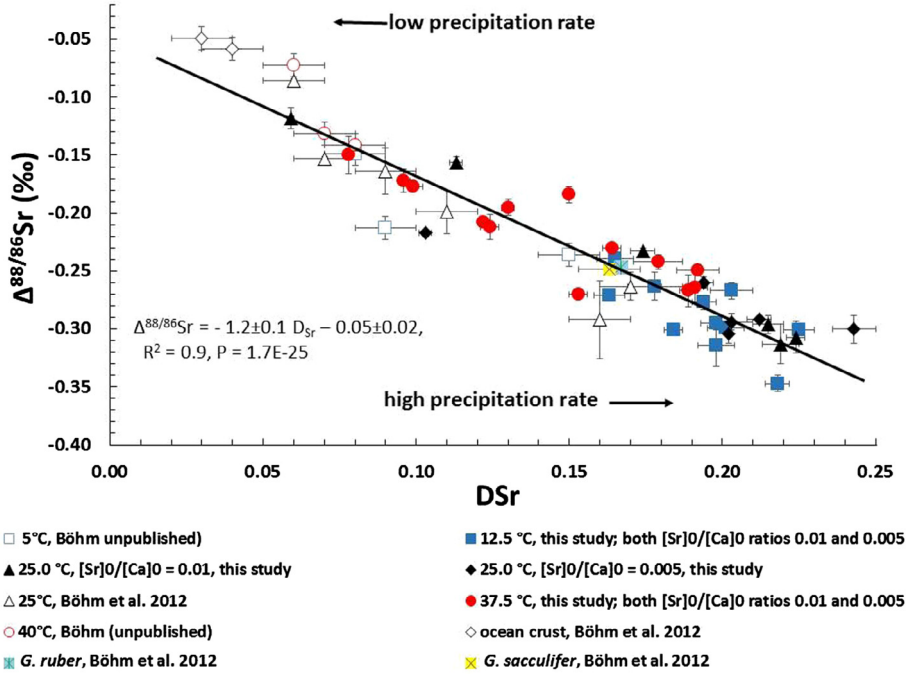

Fig. 8. Linear correlation between $\Delta^{88/86}Sr_{calcite\text{-}aq}$ and D_{Sr} for all temperatures in this study, compared with some unpublished data (courtesy of Dr. Florian Böhm) of inorganic precipitated calcite at 5 and 40 °C and values of Böhm et al. (2012) which includes results of inorganic precipitated calcite at 25 °C, calcites from ocean crust basalts and two species of planktic foraminifera (*Globigerinoides ruber* and *Globigerinoides sacculifer*). It can be seen that our result are in good agreement with literature values. Note: The solid line represents the average value of all data points in the figure.

tions of Lemarchand et al. (2004) at 20 ± 1 °C. Whereas the record at 37.5 °C resemble the earlier measurements of Tang et al. (2008b). However, there is one critical point marked by an arrow in Fig. 9b. This point is not falling along a linear line with the other points. Even more, extrapolating this single point to the rest of the data an inverse relationship between R^* and Ca fractionation could be assumed liked at 37.5 °C. At higher rates above ~3.6 μmol/m^2·h the influence of temperature on the $\Delta^{44/40}Ca_{calcite\text{-}aq}$ values are minor whereas at lower rates below about ~3.6 μmol/m^2·h Ca isotopic fractionation largely depend on temperature with much more negative values for low temperature and higher values for higher temperatures (Fig. 9d).

4. DISCUSSION

4.1. Strontium incorporation in calcite

Although not seen for the 12.5 °C data set for the higher temperatures at 25.0 and 37.5 °C we observe a non-linear behavior where the D_{Sr} values approach plateaus for relatively high and low R^* (Fig. 6). In the surface entrapment model of Watson (2004) it is assumed that the trace element and isotope ratios reflect the fluxes of ions and isotopes from the liquid toward the solid and from the solid toward the liquid. It is suggested that the growing crystal will have the composition of its surface unless diffusion of trace metal ions from its interior toward the fluid–solid transition competes with the uptake of Sr from the fluid during growth. Away from chemical equilibrium conditions ($R^* \approx 0$) and for all temperatures (see Fig. 6) as R^* increases more Sr will become incorporated. However, at very slow rates almost approaching equilibrium the diffusion rate toward the fluid–solid transition is high enough to maintain a chemical equilibrium with the input flux characterized by a distinct value (D_{Sreq}). We estimate the equilibrium D_{Sreq} at 25.0 °C ≈ 0.06 (log $D_{Sreq} \approx -1.22$) and at 37.5 °C ≈ 0.09 (log $D_{Sreq} \approx -1.05$), respectively. Latter values are slightly larger than those estimated earlier by Tesoriro and Pankow (1996) who estimated D_{Sreq} to be 0.021 ± 0.003 at 25 °C, in Lorens (1981) and to be 0.027 ± 0.011 and 0.034 as well as 0.039 at 40 and 98 °C in Katz et al. (1972) respectively. However, our D_{Sreq} value for the 25 °C experiment of 0.06 fits quite well into the predicted range of values (0.020–0.07) estimated by DePaolo (2011) depending on the conditions of the precipitating solution. Note, below an R^* of ~3.6 μmol/m^2·h there is an increasing superimposing effect of T on R^* causing the log D_{Sr} values to deviate from each other to a larger extend.

At relatively high R^* D_{Sr} remains constant (D_{SrF}) which equals K_f in the DePaolo (2011) publication. At this steady state for 25.0 °C we estimate D_{SrF} (K_f) to be ≈0.24 (log

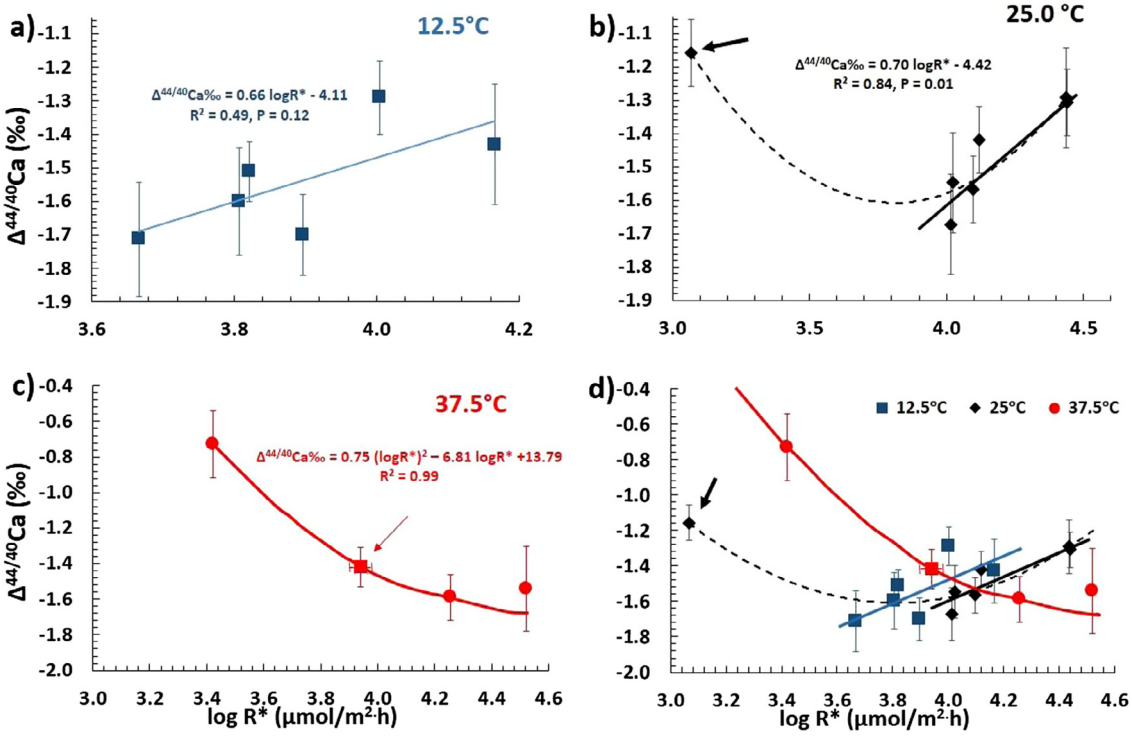

Fig. 9. The $\Delta^{44/40}Ca_{calcite\text{-}aq}$-values are plotted as function of log R^*(μmol/m^2·h) at 12.5 and 25.0 °C, respectively. As rate increase $\Delta^{44/40}Ca_{calcite\text{-}aq}$ become more positive ($\|\Delta^{44/40}Ca_{calcite\text{-}aq}\|$ decrease). It should be noted that the point marked in Fig. (b) and (d) with an arrow at about 3.1 μmol/m^2·h of the 25 °C experiment can't be excluded because repeated measurement confirmed its reproducibility. In contrast, at 37.5 °C, as R^* increases $\Delta^{44/40}Ca_{calcite\text{-}aq}$ values become more negative ($\|\Delta^{44/40}Ca_{calcite\text{-}aq}\|$ increase). The square point marked with an arrow in (c) is the average value of points 22B, 23C and 23D presented in Table 5. Fig (d) summarizes the measurement emphasizing the role of temperature. Above a threshold value of ~3.6 μmol/m^2·h a temperature effect is negligible. However, below the threshold value temperature effect is significant the lower the temperature the lower are the $\Delta^{44/40}Ca_{calcite\text{-}aq}$ values the higher the amount of isotope fractionation $\|\Delta^{44/40}Ca_{calcite\text{-}aq}\|$.

$D_{SrF} \approx -0.62$) as can be seen from Fig. 6b. Latter value is in agreement with the estimation for K_f of DePaolo (2011) to be 0.24 at 25.0 °C. In Fig. 6c we calculated $D_{SrF} \approx 0.19$ ($\log D_{SrF} \approx -0.72$) for the 37.5 °C experiment.

We compared our results of $\log D_{Sr}$ versus $\log R^*$ (μmol/m^2·h) at 25.0 °C with the model data of DePaolo (2011) which is the dashed line in Fig. 6b. The parameters of the DePaolo model are: $(R_b) = 2160$ (μmol/m^2·h) which is held constant in the DePaolo model and considered the dissolution rate of calcite in pure water at 25.0 °C. The net R^* (R_p) in the DePaolo model (R^* in our study) correspond to a range of values from 32 to 100.000 μmol/m^2·h as it can be seen from Fig. 6b. For calculation we took D_{Sreq} (K_{eq}) = 0.06 ($\log$ (−1.2) in Fig 6b) which we extrapolated from our experimental results and D_{SrF} (K_f) = 0.24 ($\log$ (0.24) ≈ −0.62 in Fig. 6b). It can be seen from Fig. 6b that our results are in general accord with DePaolo model.

4.2. Calcium and strontium isotopic fractionation in calcite

The discrepancy of the results in the Lemarchand et al. (2004) and Tang et al. (2008) data have been raised earlier (DePaolo, 2011; Nielsen et al., 2012; Watkins et al., 2013). In order to explain the discrepant observation these authors pointed toward the formation/precipitation of ACC as a possible cause for the observed differences in the fractionation behavior. In particular the Lemarchand et al. (2004) experiment favored the formation of ACC in contrast to the Tang et al. (2008) experiment. Similar to Lemarchand et al. (2004) the experiments performed in this study also favor the precipitation of ACC at higher temperatures. Hence, we may not exclude that the observed Ca isotope fractionation may also be due to the formation of ACC according to the arguments put forward in particular in Nielsen et al. (2012).

Furthermore, the transition from spiral growth to 2D nucleation may have a significant influence on the fractionation of $\delta^{44/40}$Ca (Nielsen et al., 2012). However, our data show that spiral (dislocation driven) growth mechanism is totally excluded since $SI_{calcite} > 0.34$ (Table 5, column 6) for all sample reactions. However 2D nucleation mechanism is still theoretically possible since $\Omega_{calcite} > 0.43$ Teng et al. (2000).

In order to provide an alternative explanation and model to reconcile the discrepant observations we may also assume that at lower temperatures up to about 25 °C NH_3 complexes with Ca^{2+} to form a Ca^{2+}-NH_3-aquacomplex by a coordinate covalent bonding (Fig. 10). The formation constant of this reaction ($K_{formation} = ([CaNH_3]^{2+}/[NH_3][Ca^{2+}])$ is about one (Bjerrum, 1941; Seward, 1954). We calculated the average fraction of Ca^{2+}-ions bonded to NH_3 is 0.60 ± 0.07 NH_3-ligands per Ca^{2+} in our experimental conditions based on the experimental results of Seward (1954). In order to reach a minimum oscillation potential between Ca^{2+} and NH_3 the covalent bonding of the Ca^{2+}-NH_3-aquacomplex prefers the isotopically heavy Ca-isotopes where the bonding energy (c.f. Criss (1999)) is inversely related to the isotope mass ($\Delta E \approx 1/m$). In this case relatively more light Ca isotopes are statistically available to leave the coordinated complex to become incorporation into the $CaCO_3$ lattice. Whereas relatively more heavy Ca^{2+}-isotopes remain complexed and dissolved in solution. At a certain relatively low temperature and R^* the $\Delta^{44/40}Ca_{calcite\text{-}aq}$ value is low because more light Ca isotopes are available for incorporation into the calcite lattice. However, increasing the HCO_3^- concentration and hence R^*, respectively, will shorten the mean free path travel time (Rohlf (1994)) between ions. This increases the internal energy of the system allowing relatively more heavy Ca isotopes to overcome the binding energy of the Ca^{2+}-NH_3-aquacomplex to eventually become incorporated into the calcite lattice. Hence, $\Delta^{44/40}Ca_{calcite\text{-}aq}$ correlates positively to the calcite R^*. This type of fractionation was observed in Lemarchand et al. (2004) already at about 20 °C and is in general accord with our observations at 12.5 and 25 °C, respectively.

However, increasing the temperature to about 37.5 °C eventually water molecules will replace NH_3 and solvate the Ca^{2+}-ions. Hence at a certain temperature above ~25 °C there is a transition from a Ca^{2+}-NH_3-aquacomplex to a Ca^{2+}-H_2O-aquacomplex (Irving and Williams (1953)). In this regard, we may speculate that the temperature range around 25 °C marks the transition from Ca^{2+}-NH_3 to Ca^{2+}-H_2O complexation. Probably, at low R^* the transition from the Ca^{2+}-NH_3 to Ca^{2+}-H_2O already occurs at 25 °C as indicated by one data point in Fig 9b but not at the higher R^*. Definitely our conceptual model presented here this is still speculation considered to be preliminary until final verification.

In contrast to the Ca^{2+}-NH_3-aquacomplex we infer that the bonding between the Ca^{2+}-ion and the H_2O-molecules is a weak electrostatic (van der Waals) bonding

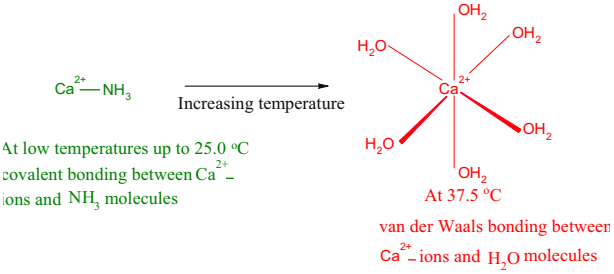

Fig. 10. Schematic illustration of our conceptual model. At and below ~25 °C the Ca^{2+}-ions form a Ca^{2+}-NH_3-aquacomplex with a relative strong covalent bonding between Ca^{2+} and NH_3. This type of bonding is following isotope equilibrium type fractionation where the heavier isotope is preferred for bonding related to a low potential oscillation energy. Hence, the lighter isotopes are statistically more available for precipitation in $CaCO_3$. However, with increasing rate and increasing internal energy more heavy isotopes are statistically available then leading to a positive R^*-$\Delta^{44/40}Ca_{calcite\text{-}aq}$ relationship. In contrast above a temperature of ~25 °C (e.g. at 37.5 °C) the Ca^{2+}-NH_3-aquacomplex is replaced by a Ca^{2+}-H_2O-aquacomplex which is formed by a relatively weak van-der-Waals bonding. In latter case only the reaction velocity matters preferring the isotopically lighter Ca^{2+}-ions (kinetic isotope fractionation). As a function of higher internal energy and precipitation rates more and more lighter isotopes are statistically incorporated forming an inverse rate-$\Delta^{44/40}Ca_{calcite\text{-}aq}$ relationship.

considerably different from the covalent bonding. In particular this means that the equilibrium between the strong distracting electrostatic forces of the protons and the attracting nuclear forces do not play any distinct role anymore. In the absence of these forces causing covalent bonding the only process being able to fractionate ions is the kinetic velocity of the ions and the chemical reaction itself. This means the higher the internal energy and R^* the higher is the discrimination between light and heavy isotopes. Having the same amount of energy the lighter isotope is simply traveling faster than the heavier one ($v \approx \sqrt{(2 \cdot \Delta E/m)}$). This results in an enrichment of lighter isotopes in the product as a function of increasing rate (the $\Delta^{44/40}Ca_{calcite\text{-}aq}$-value decreases but the amount $\|\Delta^{44/40}Ca_{calcite\text{-}aq}\|$ increases). The temperature effect on $\Delta^{44/40}Ca_{calcite\text{-}aq}$ is almost insignificant in the range between 12.5 and 25.0 °C and an R^* above ~3.6 μmol/m^2·h. The influence of temperature may become more obvious at lower rates of reaction (<3.6 μmol/m^2·h) when the temperature is raised to 37.5 °C (Fig. 9d).

Our alternative explanation offered here to explain the change of slope as a function of temperatures for the discrepancy between Lemarchand et al. (2004) and Tang et al. (2008) is based on a difference in the preferred complexation of Ca in solution as a function of temperature. Tang et al. (2008) reported the opposite trend to the Lemarchand et al. (2004) data at all temperatures of 5, 25 and 40 °C. In particular, the 40 °C dataset did not show the trend described here for the weak electrostatic explanation although also NH_3 has been in the solution. Latter discrepancy is most likely simply based on [NH_4Cl] which was set to 5 mM in the Tang et al. (2008) experiment in contrast to our solution set to 395 mM (similar to Lemarchand et al. (2004)) and about a factor of 80 higher than in the Tang et al. (2008) approach. Hence, in our solution the [Ca]:[NH_3] ratio is about one and the effect can be expected to be seen.

Multiple recent studies (c.f. Nielsen et al., 2012) have demonstrated that the [Ca]:[HCO_3^-] ratio in solution influence R^*. Hence some influence of this potential effect on both R^* and either Ca- or Sr isotope fractionation should be recognized. In our study for all data the [Ca]:[DIC] ratio which we take to represent [HCO_3^-] in the solution range between 0.66 and 2.41, with an average ratio of ~1.54. As seen from Fig 11 we do recognize an inverse trend ($n = 34$, $r = -0.3$, $p = 0.09$) between [Ca]:[DIC] and R^* which is not significant on the $p = 0.05\%$ but on the $p = 0.1\%$ level. Note, that the inverse relationship for the 12.5 °C data alone is significant.

Concerning the [Ca]:[DIC] to $\Delta^{44/40}Ca_{calcite\text{-}aq}$ relationship taking all data available into account no statistically significant relationship exists. However, for the 12.5 °C data set there is a significant [Ca]:[DIC] to $\Delta^{44/40}Ca_{calcite\text{-}aq}$ correlation ($n = 6$, $r \sim -0.9$, $p = 0.02$). We speculate that the switch of dependency of the [Ca]:[DIC] ratio of the 12.5 °C data set to the $\Delta^{44/40}Ca_{calcite\text{-}aq}$ values in contrast to the 25 and 37.5 °C data may reflect the switch from a Ca^{2+}-NH_3 to a Ca^{2+}-H_2O dominated complex system.

A similar effect of changing slopes at different temperatures is not observed for the Sr isotopes. Probably because of its lower ionic potential based on the larger ionic radius

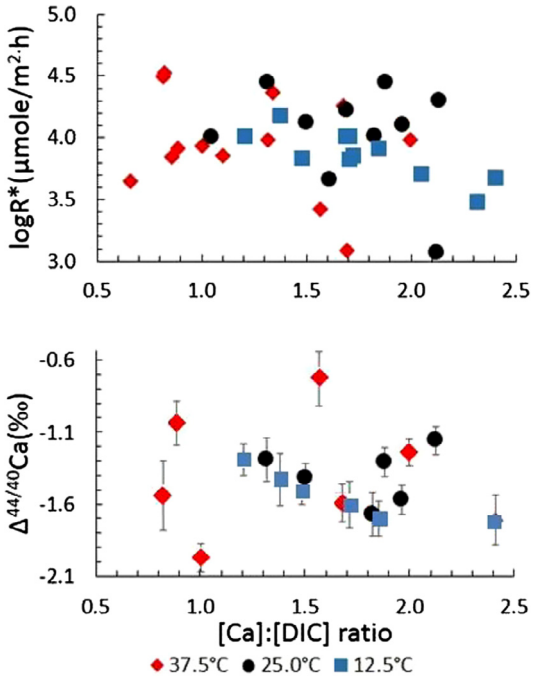

Fig. 11. Effect of [Ca]: [DIC] ratio on both precipitation rate and $\Delta^{44/40}Ca_{calcite\text{-}aq}$. It can be seen that the [Ca]:[DIC] ratio is independent of R^* for all temperatures. Similar the $\Delta^{44/40}Ca_{calcite\text{-}aq}$ ratios are independent of the [Ca]: [DIC] ratios in the 12.5 and 25 °C experiments. However, there is an inverse [Ca]: [DIC] – $\Delta^{44/40}Ca_{calcite\text{-}aq}$ relationship which is probably related to the switch from the Ca^{2+}-NH_3- to the Ca^{2+}-H_2O-aquacomplex system.

(Sr^{2+}~132 pm; Ca^{2+} ~114 pm) solvation of Sr with water molecules is more dominant than the formation of covalent bonding with NH_3 during solvation. Furthermore, it is also well known that Sr is not complexing with most ligands due its lower ionization potential when compared to Ca (Irving and Williams (1953)). In this case only kinetic fractionation is observed like for Ca at 37.5 °C.

In this regard as rate increase more lighter Sr isotopes will incorporated into calcite and $\Delta^{88/86}Sr_{calcite\text{-}aq}$ decreases ($\|\Delta^{88/86}Sr_{calcite\text{-}aq}\|$increase). The presence of $\Delta^{88/86}Sr_{calcite\text{-}aq}$ plateaus at lower and higher R^* values do not necessarily imply equilibrium type fractionation but can also be reached by kinetic fraction as modeled by DePaolo (2011). Following the DePaolo (2011) model the lower plateau is reached because the backward reaction is dominating the process whereas the higher plateau is reached because the forward reaction is becoming more dominating.

5. IMPLICATIONS

One major implication of the results of this study is that the chemical composition of the bulk solution has a major influence on the Ca isotope composition of the precipitates. Latter observation may be used to study the kinetics of solute complexation in more detail.

The finding that there is a strong inverse D_{Sr}-$\Delta^{88/86}Sr_{calcite\text{-}aq}$ relationship just depending on R^* has major implications for the marine paleo-sciences because

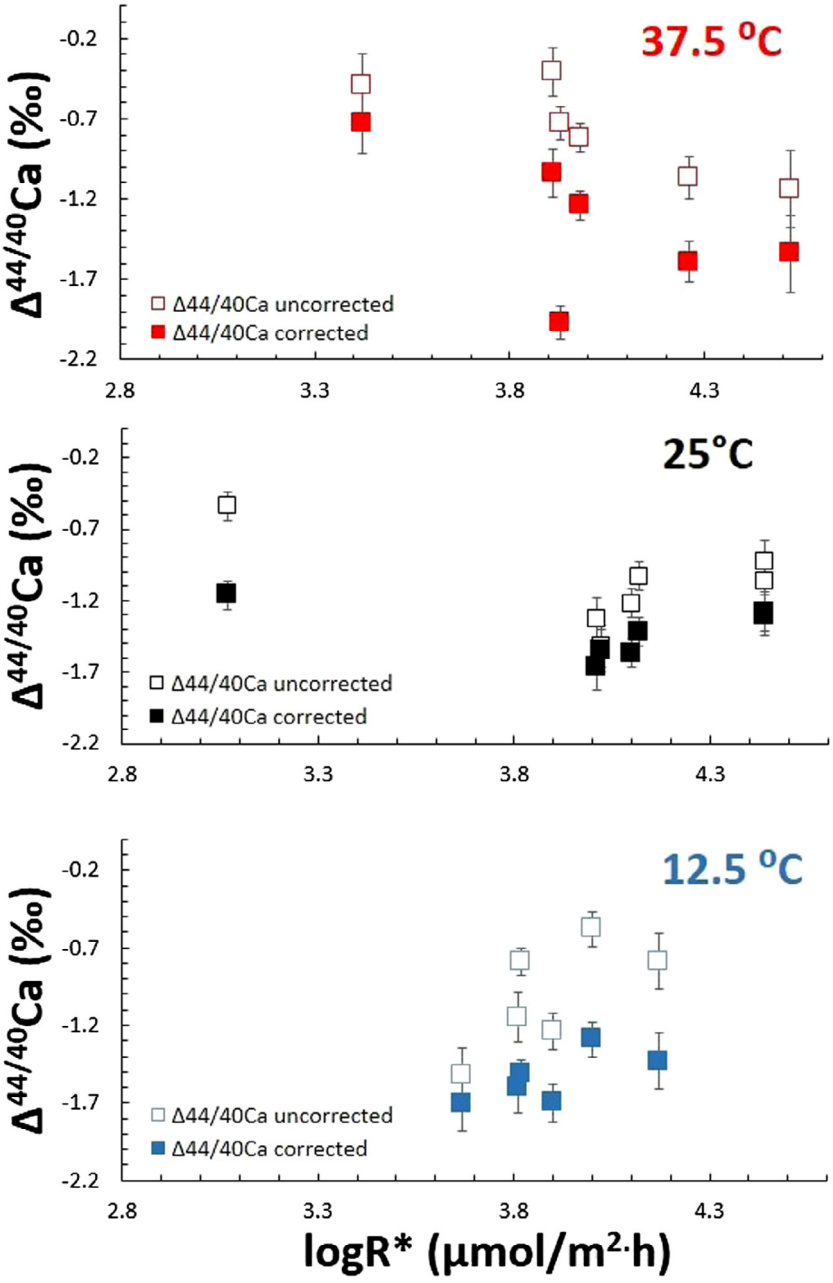

Fig. A1. This figure shows both uncorrected and corrected Ca values for the reservoir effect. Corrected values are systematically lower than the original values because bulk solution will become isotopically heavier as a function of the precipitated amount of $CaCO_3$.The maximum correction is in the order ~0.5‰ and tend to be larger for the 37.5 and 12.5 °C experiment but smaller for the 25 °C experiment.

latter observation may also be applied as a self-consisting criterial for chemical diagenesis and alteration. This is because any original D_{Sr}-$\Delta^{88/86}Sr_{calcite\text{-}aq}$ pair of data must fall along the line as seen from Fig. 8.

Temperature dependency for both Ca- and Sr-isotopes only matters for low R^* (<3.5 µmol/m^2·h) whereas for higher rates the influence of temperature diminishes. This implies that the $\Delta^{88/86}Sr_{calcite\text{-}aq}$ values in carbonate are less suited for paleo-temperature reconstructions.

The finding that the order of reaction for [HCO_3^-] changes as a function of increasing temperature from three to one, respectively, implies that at lower temperatures [HCO_3^-] has a much stronger influence on R^* than [Ca].

6. SUMMARY

- The mechanism of calcite precipitation is T and R^* dependent, the order of reaction with respect to Ca^{2+} ions is first order while the order with respect to HCO_3^- changes from 1 via 2 to 3 as temperature decrease from 37.5 via 25.0 to 12.5 °C, respectively.

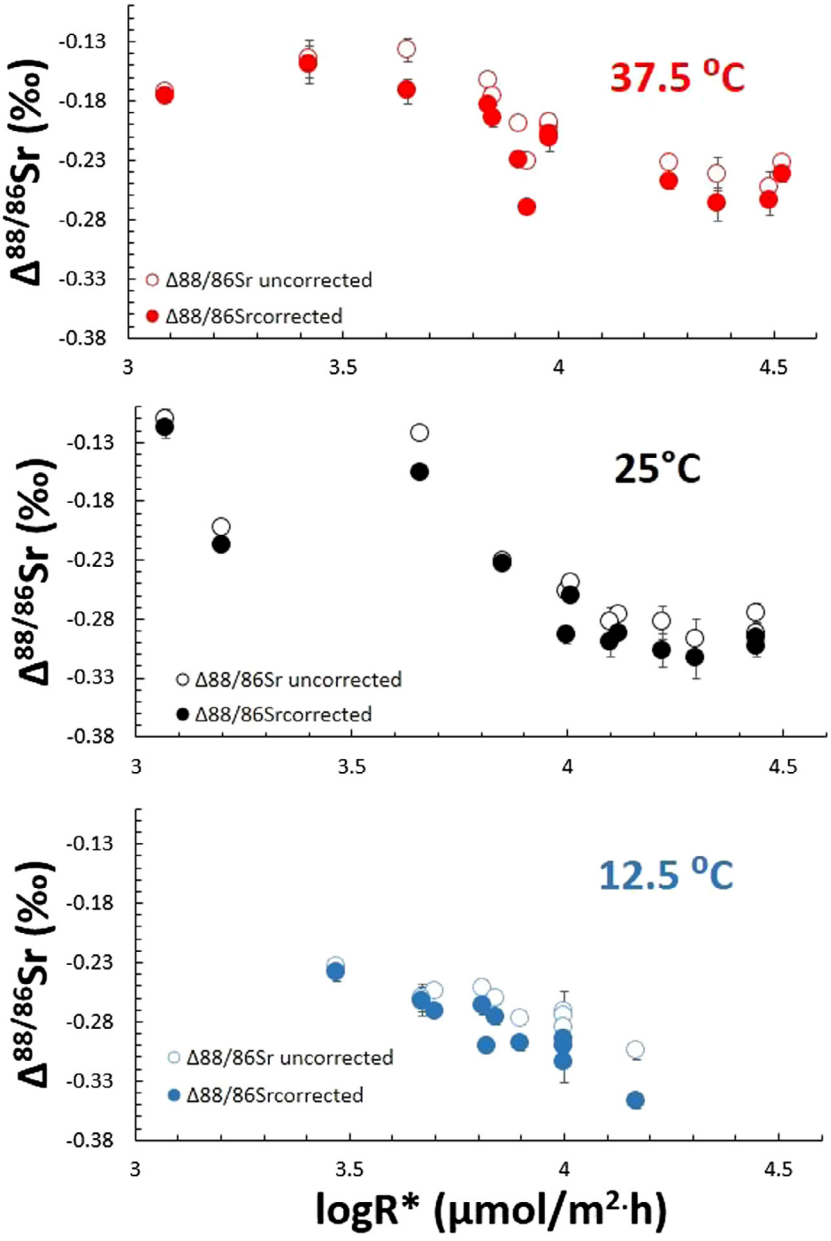

Fig. A2. Reservoir effect correction for the Sr isotope values similar to the Ca isotopes as shown above. Reservoir effect correction for Sr isotopes is much smaller when compared to Ca because the amount of Sr co-precipitating with Ca is relatively small and tend to be smaller than ~0.02‰.

- Strontium incorporation in calcite increase with increasing R^* but decrease with increasing temperature. However, the sensitivity of the temperature-D_{Sr} relationship strongly depend on R^* and is largest for lower rates.
- Strontium isotope fractionation during the precipitation of calcite is controlled by kinetic processes only. There is no influence of chemical complexation visible as for the Ca isotopes. This is probably because of Srs′ lower ionic potential solvation dominated by H_2O molecules only.
- Ca isotope fractionation depend on the complexation with either NH_3 or H_2O switching between equilibrium type like isotope fractionation as seen earlier from Lemarchand et al. (2004) and a kinetic type like fractionation as seen by Tang et al. (2008b).
- At constant rate for both Sr and Ca isotopes their fractionation factors $\Delta^{88/86}Sr_{calcite\text{-}aq}$ and $\Delta^{44/40}Ca_{calcite\text{-}aq}$ become more positive but $\|\Delta^{88/86}Sr_{calcite\text{-}aq}\|$ as well as $\|\Delta^{44/40}Ca_{calcite\text{-}aq}\|$ decrease as temperatures increase.
- An important conceptual observation is that the effect of temperature and rate are decoupled. While the temperature sets the initial conditions of Sr and Ca elemental discrimination and isotope fractionation R^* modifies this initial value accordingly. The temperature – D_{Sr} relationship is most sensitive for lower R^* (<3.5 µmol/m^2·h).
- Our inferences concerning Ca and Sr elemental and isotope fractionation are based on a limited range of R^* (~3 to 4.5 µmol/m^2·h), whereas the Lemarchand et al.

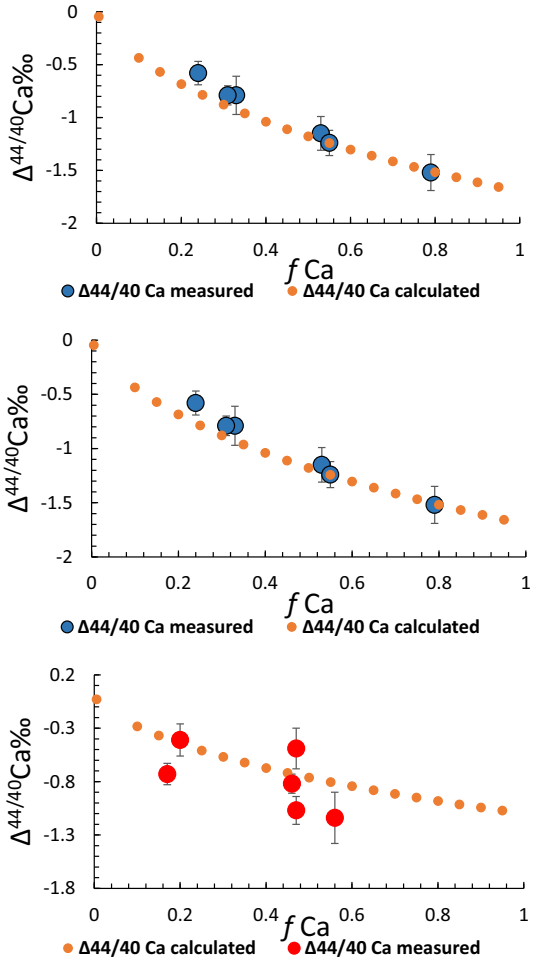

Fig A3. This figure shows the comparison of arbitrarily selected measured Ca isotope data with theoretical predictions concerning Rayleigh type precipitation of $CaCO_3$. It can be seen that theoretical predictions and experimental data are in general accord. This indicates that the data measured indeed follow Rayleigh type fractionation behavior and may become corrected as described in this study. The values for the theoretical prediction have been calculated as follows: At 12.5 °C sample 39A: the value is taken right after the linear part (accumulated product to be 79%, corresponding to $f = 0.79$) and a corresponding $\Delta^{44/4}Ca$ of −1.71 ($\alpha = 0.9983$). At 25 °C sample 7: using $\alpha = 0.9985$ corresponding to $\Delta = -1.52$ of sample 7 of the highest f ($f = 0.97$). At 37.5 °C sample 48D: $\alpha = 0.9989$ corresponding to $\Delta = -1.14$ of the highest f ($f = 0.56$).

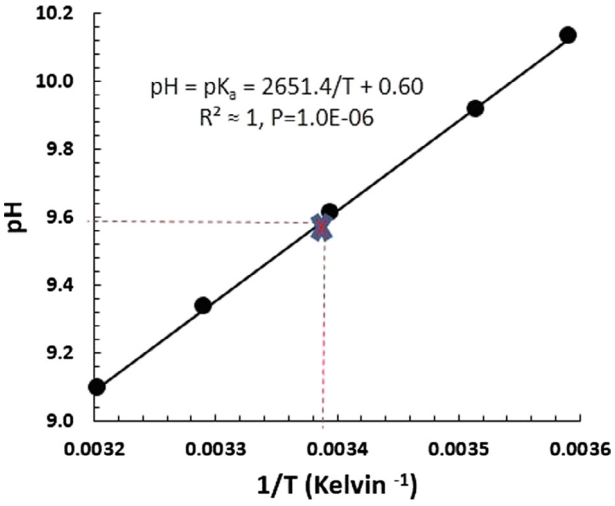

Fig. A4. pH of half neutralized mother solution versus different 1/temperatures (°K). For example, from the upper figure at 22 °C (295.15 K corresponding to 0.00339 1/°K), $pH = pK_a = 9.59 \pm 0.07$.

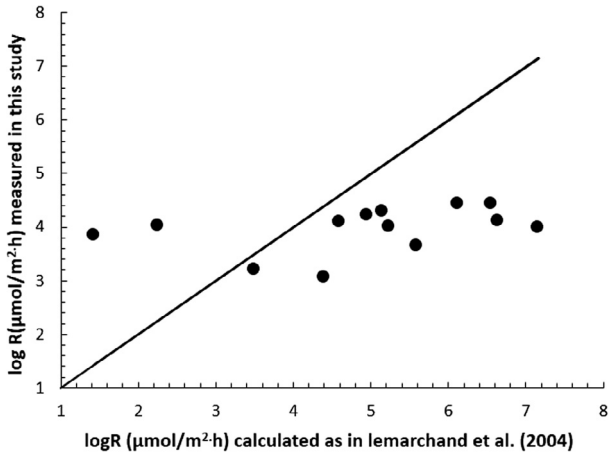

Fig. B. Measured R^* (µmol/m^2·h) using the initial rate method versus estimated R^* using Eq. (20) which was adopted earlier by Lemarchand et al. (2004) to estimate precipitation rate of their calcite products.

(2004) and the Tang et al. (2008) experiments include calcite R^* down to ~2 µmol/m^2·h. In addition, we observed that the chemical composition e.g. changes of the initial Sr/Ca ratio Sr/Ca_0 may influence chemical participation and isotope fractionation. Therefore we are fully aware that we are possibly not capturing the full range of Sr and Ca behavior during calcite precipitation, and that significant discrepancies to those observed in this study may be expected under higher or lower R^*.

ACKNOWLEDGEMENT

Three anonymous reviewers are acknowledged for their detailed reviews which significantly helped to improve the manuscript. This study is part of the TRION project in the frame of the "Trilateral Programm der Deutschen Forschungsgemeinschaft, DFG (Ei272/30-2)". Ana Kolevica is acknowledged for Laboratory help and support in the design of the experiment. For fruitful discussions, Florian Böhm, Volker Liebetrau and Jan Fietzke are acknowledged. Prof. Dr. Mutaz AlQutob from the AlQuds University in AbuDis, Palestinian Authority, is acknowledged for his general support of the work of MA.

APPENDIX A

A1. Correction for isotope fractionation due to the reservoir effect

The isotope composition of an aquatic reservoir with respect to Ca and Sr will change when a significant amount of Ca and Sr is precipitating as solid $CaCO_3$. This has to be corrected for:

Isotope fractionation (I) $\alpha_{pr} = R_p/R_r$

where p and r are the product and the reactant respectively and R is the abundance of the heavy isotope; R = heavy isotope/light isotope

While (II) : $\Delta \approx (\alpha - 1) * 1000$

Rearranged to (III): $\alpha \approx (\frac{\Delta}{1000} + 1)$

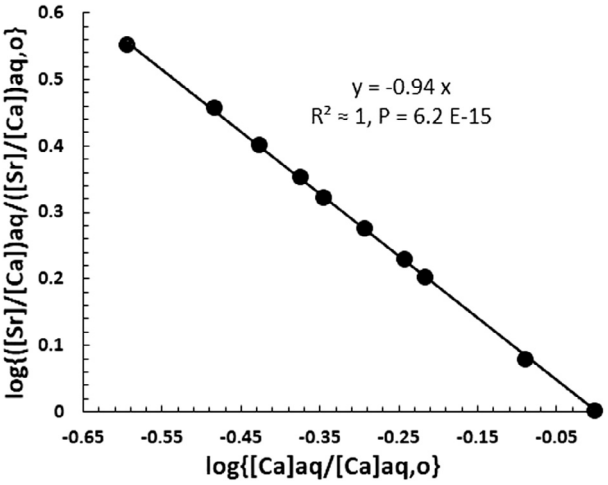

Fig. C. Determination of D_{Sr} of arbitrarily selected sample reaction 2 at 25.0 °C graphically by plotting of $\log\{[Ca]_{aq}/[Ca]_{aq,o}\}$ versus $\log\{([Sr]/[Ca])_{aq}/([Sr]/[Ca])_{aq,o}\}$. The slope of this curve equals $D_{Sr} - 1$ and results in $D_{Sr} = 0.06$ being close to (0.059) as value calculated from (Eq. (21)) and shown in Table 5. This figure is a validation of the Usdowski (1975) equation to our experimental system of precipitation reactions in order to calculate D_{Sr}.

Table A
Acid dissociation constant (pK_a) of ammonium chloride as function of temperature.

Temperature °C	Temperature °K	1/T (°K^{-1})	$pH = pK_a$
5.3	278.45	0.003591	10.130
11.4	284.55	0.003514	9.915
21.4	294.55	0.003395	9.611
30.7	303.85	0.003291	9.335
39.0	312.15	0.003204	9.095

Note: The pH values at different temperatures of half neutralized mother solution for calcite: $K_a = [NH_3]\cdot[H^+]/[NH_4^+]$, at half neutralization $[NH_3] = [NH_4^+]$ and so $K_a = [H^+]$ and $pK_a = pH$. Using van't Hoff equation: $-\ln K_a = [\Delta H/RT] + C$; or $pK_a = pH = [\Delta H/2.303RT] + C$, where R is the gas content = 8.314 J/mol. Kelvin, T is the temperature in Kelvin and °C is constant.

Substituting Eq. (I) in Eq. (III) results in (IV): $R_p/R_r = (\frac{\Delta}{1000} + 1)$

The Eq. 3.1.17 from Zeebe and Wolf-Gladrow, 2003 accounts for the Rayleigh distillation effect:

(V) $R_p/R_r = (f^{\alpha} - 1)/(f - 1)$; f is the fraction of metal ions remaining in solution.

Eqs. (V) and (IV) result in: $(\frac{\Delta}{1000} + 1) = (f^{\alpha} - 1)/(f - 1)$

Rearrange to (VII): $f^{\alpha} = \frac{\Delta f}{1000} + f - \frac{\Delta}{1000}$

Eq. (VII) can be rewritten to (VIII): $\alpha \ln f = \ln [\frac{\Delta f}{1000} + f - \frac{\Delta}{1000}]$

Eq. (VIII) is then arranged to Eq. (7) as in the text: $\alpha_{corrected} = (ln[\frac{\Delta f}{1000} + f - (\frac{\Delta}{1000})])/lnf$

A correction for the "reservoir effect" is considered when the reservoir (bulk solution) is not infinite rather than relatively small compared to the amount of solid material precipitating out of this reservoir (Fruchter et al., 2016; Böhm et al., 2012). Given a kinetic isotope fractionation where the light isotopes are enriched in the solid the reservoir becomes enriched in the heavy isotope. Latter value deviates from an infinite reservoir as a function of the relative amount precipitated from the solution. The isotope values measured in the solid precipitated from a restricted reservoir would then tend to show higher values to those values precipitated from an infinite reservoir. From Figs. A1 and A2) the corrected and uncorrected values for Sr and Ca isotopes, respectively, are plotted to illustrate the correction applying Eqs. (7) and (8). The reservoir correction is actually quite small o negligible for Sr (Fig. A2) because only a small fraction of Sr co-precipitated with Ca. In this regard for Sr the reservoir is almost infinite. In contrast corrections are larger for Ca because a significant amount of Ca precipitated out of solution. Correction for the reservoir effect (Table 5, columns 13 to 18) leads to an increase of the measured values in to a maximum of ~0.5‰, respectively.

A2. K_a of ammonium ion and DIC calculations

Total alkalinity (TA, see Eq. (a1)) was measured from neutralization titration with 0.02 N HCl at different intervals of time during the course of precipitation for some reactions. We found that TA did not increase more than 10% from the value at the precipitation point until the end of the reaction (see Fig. 2). We therefore determined TA at the end of all the reactions and adopted this value for further calculations.

$$TA = [NH_3] + [HCO_3]^- + 2[CO_3^{2-}] \quad (a1)$$

$[NH_3]$ in our solutions at different results is calculated following Lemarchand et al. (2004):

Table B
Ksp values of calcite, ACC and $SrCO_3$ as function of temperature and salinity.

T/°C	$Ksp_{calcite} * 10^7$	$Ksp_{ACC} * 10^7$	$Ksp_{SrCO3} * 10^{10}$
37.5	3.72	6.17	4.98
25.0	3.74	9.09	5.36
12.5	3.85	13.85	5.24

Table C
Estimated R^* using Eq. (20) for samples precipitated at 25 °C versus measured R^* values.

Sample reaction	log $[CO_3^{2-}]$ (mM)	Log R (μmol/m^2·h) calculated as in Lemarchand et al. (2004)	log R (μmol/m^2·h) measured in this study
43C	0.09	6.55	4.44
43D	0.27	7.16	4.00
44A	−0.04	6.12	4.44
44B	0.12	6.64	4.12
45C	−0.33	5.14	4.30
45D	−0.30	5.23	4.01
46E	−0.39	4.95	4.22
46F	−0.49	4.59	4.10
2	−0.55	4.39	3.07
3	−0.19	5.59	3.66
4	−0.82	3.49	3.20
7	−1.40	2.25	4.02
8	−1.70	1.43	3.85

Note: Equation used by Lemarchand et al. (2004) to calculate rate is $\log R^* = n_2 \log([CO_3^{2-}]) + \log k_f$, where for samples 43C to 4: $n_2 = 3.34$ and $\log k_f = 6.24$. For samples 7 and 8: $n_2 = 2.73$ and $\log k_f = 6.07$.

$$[NH_3] = \frac{[Cl^-] + TA - 2[M^{2+}]}{\frac{[H^+]}{K_a} + 1} \quad (a2)$$

where $[M^{2+}]$ is the concentration of metal divalent ions in the solution, $[Cl^-]$ is the concentration of chloride ions, $[H^+]$ calculated from pH values at the end of each experiment and K_a is the ammonium acid dissociation constant.

The acid dissociation constant (pK_a) of ammonium chloride (Eq. (a3)) equals the pH of the half neutralized mother solution, because at half neutralization the concentrations of ammonia species are equal and K_a equals $[H^+]$. Measured values of pK_a at different temperatures are shown in Table A.

$$[NH_4^+]_{(aq)} \rightleftharpoons NH_{3(aq)} + H^+_{(aq)} \quad (a3)$$

By plotting pH versus 1/T (Fig. A4) we can calculate pK_a at any temperature as well as the apparent enthalpy of ionization of ammonium which is calculated to be about +51 kJ/mol.

$[CO_3^{2-}]$ in our solutions also calculated following Lemarchand et al. (2004): (Eq. (a4)).

$$[CO_3^{2-}] = \frac{TA - [NH_3]}{\frac{[H^+]}{K_2} + 2} \quad (a4)$$

where K_2 is the second dissociation constant of carbonic acid and calculated following Millero (1995): (Eq. (a5))

$$\ln K_2 = -0.84 - 3741.13/T - 1.44\ln(T) + (-0.13 - 24.41/T)S^{0.5} + 0.12S - 0.01S^{1.5} \quad (a5)$$

where temperature is the temperature in Kelvin (°K) and S is the salinity of the solution as determined at the end of all the reactions.

A3. Saturation indexes with respect to calcite, amorphous calcium carbonate (ACC) and strontianite ($SrCO_3$)

Saturation state $\Omega = [Me^{2+}][CO_3^{2-}]/Ksp$ (Millero (1995)), where Me^{2+} is either Ca or Sr. Saturation index (SI) = $\log \Omega \cdot K_{sp}$ of calcite is calculated as function of temperature at a salinity of 32 psu as in Millero (1995). K_{sp} of ACC is determined as in Clarkson et al. (1992) and K_{sp} of strontianite is determined as in Busenberg et al. (1984) are shown in Table B.

REFERENCES

Atkins P. and De Paulla J. (2006) Atkins, Physical Chemistry. 8th Edition, W.H. Freeman and company, New York. P 798.

Baker P. A., Gieskes J. M. and Elderfield H. (1982) Diagenesis of carbonates in deep sea sediments—evidence from Sr/Ca ratios and interstitial dissolved Sr data. *J. Sedimentary Petrol.* **52**, 71–82.

Banner J. L. (1995) Application of the trace element and isotope geochemistry of strontium to studies of carbonate diagenesis. *Sedimentology* **42**, 805–824.

Berner R. A. (2004) The Phanerozoic carbon cycle: CO_2 and O_2: Oxford University Press (in press).

Bjerrum J. (1941) Metal Ammine Formation in Aqueous Solutions. P. Haase and Son, Copenhagen, P. 147.

Böhm F., Gussone N., Eisenhauer A., Dullo W.-C., Reynaud S. and Paytan A. (2006) Calcium isotope fractionation in modern scleractinian corals. *Geochim. Cosmochim. Acta* **70**, 4452–4462.

Böhm F., Eisenhauer A., Tang J., Dietzel M., Krabbenhöft A., Kisakürek B. and Horn C. (2012) Strontium isotope fractionation of planktic foraminifera and inorganic calcite. *Geochim. Cosmochim. Acta* **93**, 300–314.

Burton E. A. and Walter L. M. (1987) Relative precipitation rates of aragonite and Mg calcite from seawater: temperature or carbonate ion control? *Geology* **15**, 111–114.

Busenberg E., Plummer L. N. and Paker V. B. (1984) The solubility of strontianite ($SrCO_3$) in CO_2-HO_2 solutions between 2 and 91 °C the association constants of $SrHCO_3^+$(aq) and $SrCO_3^0$(aq) between 5 and 80 °C and an evaluation of the thermodynamic properties of Sr^{2+} (aq) and $SrCO_3$ (cr) at 25 °C and 1 atm total pressure. *Geochim. Cosmochim. Acta* **48**, 2021–2035.

Clarkson J. R., Price T. J. and Adams C. J. (1992) Role of metastable phases in the spontaneous precipitation of calcium carbonate. *J. Chem. Soc., Faraday Trans.* **88**(2), 243–249.

Criss R. E. (1999) *Principles of Stable Isotope Distribution*. Oxford University Press.

DePaolo D. J. (2011) Surface kinetic model for isotopic and trace element fractionation during precipitation of calcite from aqueous solutions. *Geochim. Cosmochim. Acta* **75**, 1039–1056.

Fruchter N., Eisenhauer A., Dietzel M., Fietzke J., Böhm F., Montagna P., Stein M. M., Lazar B. B., Rodolfo-Metalpa R. R. and Erez J. J. (2016) $^{88}Sr/^{86}Sr$ fractionation in inorganic aragonite and in corals. *Geochim. Cosmochim. Acta* **178**, 268–280.

Gabitov R. I. (2013) Growth-rate induced disequilibrium of oxygen isotopes in aragonite: an in situ study. *Chem. Geol.*, 268–275.

Gabitov R. I., Sadekov A. and Leinweber A. (2014) Crystal growth rate effect on Mg/Ca and Sr/Ca partitioning between calcite and fluid: an in situ approach. *Chem. Geol.* **367**, 70–82.

Gagan M. K., Ayliffe L. K., Hoplry D., Cali J. A., Mortimer G. E., Chapell J., McCulloch M. T. and Head M. J. (1998) Temperature and surface ocean water balance of the mid-Holocene tropical western Pacific. Science 279, 1014–1018.

Garrels R. M. and Christ C. L. (1965) *Solutions, Minerals and Equilibria*. Freeman, Cooper and Co.

Gruzensky P. M (1967) Growth of calcite crystals. In Crystal Growth, Conference Proceedings of the International Conference on Crystal Growth (1966: Boston MA) (ed. H. Steffen Peiser), Supplement to Journal of Physics and Chemistry of Solids S: 365 Suppl. 1. Pergamon Press, New York.

Hathorne Ed. C., Gagnon A., Felis T., et al. (2013) Interlaboratory study for coral Sr/Ca and other element/Ca ratio measurements. G3 Geochem. Geophys. Geosyst., 14(9), 3730–3750.

Hemming N. G., Reeder R. J. and Hanson G. N. (1995) Mineral-fluid and isotopic fractionation of boron in synthetic calcium carbonate. *Geochim. Cosmochim. Acta* **59**, 371–379.

Heuser A., Eisenhauer A., Gussone N., Bock B., Hansen B. T. and Nägler T. F. (2002) Measurement of calcium isotopes (δ^{44}Ca) using a multicollector TIMS technique. *Int. J. Mass Spectrom.* **220**, 387–399.

Heuser A., Eisenhauer A., Böhm F., Wallmann K., Gussone N., Pearson P. N., Nägler T. F. and Dullo1 W.-C. (2005) Calcium isotope ($\delta^{44/40}$Ca) variations of Neogene planktonic foraminifera. *Paleoceanography* **20**(PA2013), 1–13.

Huang Y. and Fairchild I. J. (2001) Partitioning of Sr^{2+} and Mg^{2+} into calcite under karst-analogue experimental conditions. *Geochim. Cosmochim. Acta* **65**(1), 47–62.

Humphrey J. D. and Howell R. P. (1999) Effect of differential stress on strontium partitioning in calcite. *J. Sediment. Res.* **69**, 208–215.

Irving H. and Williams R. J. P. (1953) The stability of transition metal complexes. *J. Chem. Soc.*, 3192–3210.

Jacobson R. L. and Usdowski H. E. (1976) Partitioning of Sr^{2+} between calcite, dolomite, and liquids: an experimental study under high temperature diagenetic conditions, and a model for the prediction of mineral pairs for geothermometry. *Contrib. Miner. Petrol.* **59**, 171–185.

Katz A., Sass E., Starinsky A. and Holland H. D. (1972) Strontium behavior in the aragonite– calcite transformation: an experimental study at 40–988 C. *Geochim. Cosmochim. Acta* **36**, 481–496.

Kazmierczak T. F., Tomson M. B. and Nancollas G. H. (1982) Crystal growth of calcium carbonate. A controlled composition kinetic study. *J. Phys. Chem.* **86**(1), 103–107.

Koutsoukos P. G. and Kontoyannis C. G. (1984) Precipitation of calcium carbonate in aqueous solutions. *J. Chem. Soc., Faraday Trans.* **80**(1), 1181–1192.

Krabbenhöft A., Fietzke J., Eisenhauer A., Liebetrau V., Böhm F. and Vollstaedt H. (2009) Determination of radiogenic and stable strontium isotope ratios ($^{87}Sr/^{86}Sr$; $\delta^{88/86}Sr$) by thermal ionization mass spectrometry applying an $^{87}Sr/^{84}Sr$ double spike. *J. Anal. At. Spectrom.* **24**, 1267–1271.

Langmuir D. (1997) *Aqueous Environmental Geochemistry*. Prentice Hall.

Lea D. W., Mashiotta T. A. and Spero H. J. (1999) Controls on magnesium and strontium uptake in planktonic foraminifera determined by live culturing. *Geochim. Cosmochim. Acta* **63**, 2369–2379.

Lemarchand D., Wasserburg G. J. and Papanastassiou D. A. (2004) Rate-controlled calcium isotope fractionation in synthetic calcite. *Geochim. Cosmochim. Acta* **68**, 4665–4678.

Lopez O., Zuddas P. and Faivre D. (2009) The influence of temperature and seawater composition on calcite crystal growth mechanisms and kinetics: implications for Mg incorporation in calcite lattice. *Geochim. Cosmochim. Acta* **73**, 337–347.

Lorens R. B. (1981) Sr, Cd, Mn and Co distribution coefficients in calcite as a function of calcite precipitation rate. *Geochim. Cosmochim. Acta* **45**, 553–561.

Malone M. J. and Baker P. A. (1999) Temperature dependence of the strontium distribution coefficient in calcite: an experimental study from 40 to 200 °C and application to natural diagenetic calcites. *J. Sediment. Res.* **69**, 216–223.

Millero F. J. (1995) Thermodynamics of the carbon dioxide system in the oceans. *Geochim. Cosmochim. Acta* **59**, 661–677.

Morse J. W. and Bender M. L. (1990) Partition coefficients in calcite: examination of factors influencing the validity of experimental results and their application to natural systems. *Chem. Geol.* **82**, 265–277.

Morse J. W. and Mackenzie F. T. (1990) *Geochemistry of Sedimentary Carbonates*. Elsevier, Amsterdam.

Mucci A. and Morse J. W. (1983) The incorporation of Mg and Sr into calcite overgrowths: influences of growth rate and solution composition. *Geochim. Cosmochim. Acta* **47**, 217–233.

Nancollas G. H. and Reddy M. M. (1971) The crystallization of calcium carbonate. II. Calcite growth mechanism. *J. Colloid Interface Sci.* **37**(4), 824–830.

Nehrke G., Reichart G. J., Van Cappellen P., Meile C. and Bijma J. (2007) Dependence of calcite growth rate and Sr partitioning on solution stoichiometry: non-Kossel crystal growth. *Geochim. Cosmochim. Acta* **71**, 2240–2249.

Niedermayr A., Köhler S. J. and Dietzel M. (2013) Impacts of aqueous carbonate accumulation rate, magnesium and polyaspartic acid on calcium carbonate formation (6–40 °C). *Chem. Geol.* **340**, 105–120.

Nielsen L. C., DePaolo D. J. and De Yoreo J. J. (2012) Self-consistent ion-by-ion growth model for kinetic isotopic fractionation during calcite precipitation. *Geochim. Cosmochim. Acta* **86**, 166–181.

Paquette J. and Reeder R. J. (1990) New type of compositional zoning in calcite: insights into crystal-growth mechanisms. *Geology* **18**, 1244–1247.

Paquette J. and Reeder R. J. (1995) Relationship between surface structure, growth mechanism, and trace element incorporation in calcite. *Geochim. Cosmochim. Acta* **59**, 735–749.

Richter F. M. and Liang Y. (1993) The rate and consequence of Sr diagenesis in deep-sea carbonates. *Earth Planet. Sci. Lett.* **117**, 553–565.

Rohlf J. W. (1994) *Modern Physics from Alpha to Z^0*. Wiley.

Rosenthal Y., Boyle E. A. and Slowey N. (1997) Temperature control on the incorporation of magnesium, strontium, fluorine, and cadmium into benthic foraminiferal shells from Little Bahama Bank: prospects for thermocline paleoceanography. *Geochim. Cosmochim. Acta* **61**, 3633–3643.

Seward R. P. (1954) The Complexing of Hydrazine with Calcium Ion as Determined by Distribution Measurements. J. Am. Chem. Soc. 76(19), 4850–4852.

Smith S. V., Buddemeier R. W., Redalje R. C. and Houck J. E. (1979) Strontium-calcium thermometry in coral skeletons. *Science* **204**, 404–407.

Stoessell R. K., Klimentidis R. E. and Prezbindowski D. R. (1987) Dedolomitization of Na–Ca–Cl brines from 100 to 200 °C at 300 bars. *Geochim. Cosmochim. Acta* **51**, 847–856.

Stoll H. M. and Schrag D. P. (2000) Coccolith Sr/Ca as a new indicator of coccolithophorid calcification and growth rate. *Geochem. Geophys. Geosyst.* **1**, 1–24.

Stoll H. M., Klaas C. M., Probert I., Encinar J. R. and Alonso J. I. G. (2002a) Calcification rate and temperature effects on Sr partitioning in coccoliths of multiple species of coccolithophorids in culture. *Global Planet. Change* **34**, 153–171.

Stoll H. M., Rosenthal Y. and Falkowski P. (2002b) Climate proxies from Sr/Ca of coccolith calicte: calibrations from continuous culture of *Emiliania huxleyi*. *Geochim. Cosmochim. Acta* **66**, 927–936.

Tang J., Köhler S. J. and Dietzel M. (2008a) Sr^{2+}/Ca^{2+} and $^{44}Ca/^{40}Ca$ fractionation during inorganic calcite formation: I. Sr incorporation. *Geochim. Cosmochim. Acta* **72**, 3718–3732.

Tang J., Dietzel M., Böhm F., Köhler S. J. and Eisenhauer A. (2008b) Sr^{2+}/Ca^{2+} and $^{44}Ca/^{40}Ca$ fractionation during inorganic calcite formation: II. Ca isotopes. *Geochim. Cosmochim. Acta* **72**, 3733–3745.

Tang J., Niedermayr A., Köhler S. J., Böhm F., Kisakürek B., Eisenhauer A. and Dietzel M. (2012) Sr^{2+}/Ca^{2+} and $^{44}Ca/^{40}Ca$ fractionation during inorganic calcite formation: III. Impact of salinity/ionic strength. *Geochim. Cosmochim. Acta* **77**, 432–443.

Teng H. H., Dove P. M. and DeYoreo J. J. (2000) Kinetics of calcite growth: surface processes and relationships to macroscopic rate laws. *Geochim. Cosmochim. Acta* **13**, 2255–2266.

Tesoriro A. J. and Pankow J. F. (1996) Solid solution partitioning of Sr^{2+}, Ba^{2+} and Cd^{2+} to calcite. *Geochim. Cosmochim. Acta* **60**(6), 1053–1063.

Usdowski H. E. (1975) *Fraktionierung der Spurenelemente bei der Kristallisation*. Springer-Verlag, Berlin, Heidelberg, p. 104.

Vollstaedt H., Eisenhauer A., Wallmann K., Böhm F., FietzkeJ., Liebetrau V., Krabbenhöft A.,Farkaš J., TomašovýchA., Raddatz J. and Veizer J. (2014) The Phanerozoic $\delta^{88/86}Sr$ record of seawater: New constraints on past changes in oceanic carbonate fluxes. Geochim. Cosmochim. Acta, Volume 128, 249-265.

Watkins J. M., Nielsen L. C., Ryerson F. J. and DePaolo D. J. (2013) The influence of kinetics on the oxygen isotope composition of calcium carbonate. *Earth Planet. Sci. Lett.* **375**, 349–360.

Watson E. B. (2004) A conceptual model for near-surface kinetic controls on the trace element and stable isotope composition of abiogenic calcite crystals. *Geochim. Cosmochim. Acta* **68**, 1473–1488.

Weinbauer M. G. and Velimirov B. (1995) Calcium, magnesium and strontium concentrations in the calcite sclerites of Mediterranean gorgonians (Coelenterata: Octocorallia). *Estuar. Coast. Shelf Sci.* **40**, 87–104.

Wiechers H. N. S., Sturrock P. and Marais G. V. R. (1975) Calcium carbonate crystallization kinetics. *Water Res.* **9**(9), 835–845.

Zeebe R. E. and Wolf-Gladrow D. (2003) CO_2 in seawater, kinetics, isotopes. Elsevier Oceangraphy Series, 65.

Zuddas P. and Mucci A. (1994) Kinetics of calcite precipitation from seawater: I. A classical kinetics descriptions for strong electrolyte solutions. *Geochim. Cosmochim. Acta* **58**, 4353–4362.

Zuddas P. and Mucci A. (1998) Kinetics of calcite precipitation from seawater: II. The influence of the ionic strength. *Geochim. Cosmochim. Acta* **62**, 757–766.

Associate editor: Andrew D. Jacobson